

An Empirical Analysis of the Salient Geometric Properties of Crumpled Paper Balls in Compression

A Thesis Report

Submitted In Partial Fulfilment of the Requirements

For the Degree of

Bachelor of Engineering /Bachelor of Design in Architecture

In

Civil Engineering

By

Isaac Beton

311208290

Supervisor: Professor Andy Dong

Co-Supervisors:

Dr Emmanuel Flores-Johnson

Dr Dorian Hanaor

School of Civil Engineering

University of Sydney, NSW 2006

Australia

30th October 2015

Student Disclaimer

The work comprising this thesis is substantially my own, and to the extent that any part of this work is not my own I have indicated that it is not my own by acknowledging the source of that part or those parts of the work. I have read and understood the *University of Sydney Student Plagiarism: Coursework Policy and Procedure*. I understand that failure to comply with the *University of Sydney Student Plagiarism: Coursework Policy and Procedure* can lead to the University commencing proceedings against me for potential student misconduct under chapter 8 of the *University of Sydney By-Law 1000* (as amended).

Departmental Disclaimer

This thesis was prepared for the School of Civil Engineering at the University of Sydney, Australia, and describes an empirical investigation into the geometric and mechanical properties of crumpled paper. The opinions, conclusions and recommendations presented herein are those of the author and do not necessarily reflect those of the University of Sydney or any of the sponsoring parties to this project.

Acknowledgements

Firstly, I'd like to thank my family and friends, without whose support, encouragement, and company I would have undoubtedly been unable to persevere through neither this Thesis Project nor the final year of my Bachelor's Degree.

I'd also like to give an enormous thank you to my Thesis partner, Rebecca Tan, whose tireless and unwavering work ethic is inspirational. I'd also like to thank her for putting up with all of my various tangents and all the unnecessary times I overcomplicated things.

I believe we have both worked very hard at this project, as well as the last few years that we have been studying together, and I dearly hope you don't hate me after this year.

Further, I would like to thank our excellent supervisor, Professor Andy Dong, whom I immensely admire, respect, and enjoyed working with over the course of the year. Thank you for all of your insight, practical guidance, and taking the time to thoroughly engage with us

on a weekly basis. This has been a very enjoyable and rewarding project, so thank you very much for providing us with the opportunity to work with you.

To Doctors Emmanuel Flores-Johnson and Dorian Hanaor, thank you very much for all of your wisdom and experience, particularly in the technical and experimental aspects of this project. Without a doubt, if we had not had your expertise, we would have floundered for weeks on end. Thank you very much for taking time out of your busy schedules to sit in upon our weekly meetings and responding to any of our queries.

Lastly, I would like to thank the University and associated staff that provide and maintain all the facilities and equipment that we used during the course of this research.

1| TABLE OF CONTENTS

1 TABLE OF CONTENTS.....	4
2 ABSTRACT.....	6
3 LIST OF FIGURES.....	7
4 LIST OF TABLES.....	9
5 INTRODUCTION.....	10
6 LITERATURE REVIEW.....	12
6.1 GEOMETRY.....	12
6.1.1 EMPIRICAL.....	12
6.1.2 ANALYTICAL.....	16
6.2 MECHANICAL PROPERTIES.....	18
6.2.1 EMPIRICAL.....	18
6.2.2 ANALYTICAL.....	19
METHODOLOGY.....	22
6.3 AIM.....	22
6.4 HYPOTHESIS	22
6.5 APPROACH.....	22
6.6 SAMPLE PREPARATION.....	22
6.6.1 MATERIALS.....	22
6.6.2 SIZE	23
6.6.3 SAMPLE SIZE.....	23
6.6.4 SPECIMEN POSITIONING APPARATUS.....	23
6.6.5 LOAD TEST	24
6.6.6 3D SCANNING	24
6.6.7 3D MODEL ANALYSIS	28
6.6.8 IMAGE PROCESSING	29
6.6.9 DATA ANALYSIS	31
7 RESULTS.....	32
7.1 INITIAL REMARKS	32
7.2 DATA	33
8 DISCUSSION.....	40

8.1	PRINCIPAL ASSUMPTION	40
8.2	DISTRIBUTION OF RIDGE LENGTHS AND AREAS	41
8.3	FORCE AND ENERGY PROPORTIONALITY	45
8.4	ENERGY AS A FUNCTION OF GEOMETRY	47
8.5	LIMITATIONS AND ERRORS.....	51
8.5.1	SPECIMEN PREPARATION	51
8.5.2	TESTING.....	51
8.5.3	3D SCANNING	52
8.5.4	ELEVATION MAPPING	52
8.5.5	MATLAB.....	52
8.5.6	2D SCANNING	52
8.5.7	GRASSHOPPER IMAGE SAMPLING	53
9	CONCLUSIONS	54
10	REFERENCES.....	55
11	APPENDICES	57
11.1	MATLAB IMAGE PROCESSING CODE	57
11.1.1	WATERSHED CODE	57
11.1.2	IMRAG FUNCTION.....	59
11.2	2D EDGE DETECTION GRASSHOPPER DEFINITION	62
11.3	MANN-WHITNEY U-TESTS	63
11.4	COMPLETE PLOTS	65
11.4.1	FORCE VS DISPLACEMENT	65
11.4.2	FORCE VS COMPACTION RATIO.....	65
11.4.3	STIFFNESS VS DISPLACEMENT	66
11.4.4	STIFFNESS VS COMPACTION RATIO	66
11.5	PERIMETER PROBABILITY DISTRIBUTION	67
11.6	AREA PROBABILITY DISTRIBUTION	67

2| ABSTRACT

The simple act of scrunching up a piece of paper in frustration is a remarkable process as it is highly effective at absorbing energy for its very low mass density. Despite this being an everyday occurrence, the process is quite complex and is not yet fully understood.

This project, "*An Empirical Analysis of the Salient Geometric Properties of Crumpled Paper in Compression*" explores the relationships that exist between the mechanical properties of a crumpled paper ball and the geometric properties observed in its uncrumpled state.

Described herein are two different methods used to determine said geometric properties, the results of which are described in detail.

Particularly, the distributions of Platelet area, perimeter, adjacency, and total ridge length across six sample groups are determined and compared to prior research.

300 samples were created, 250 of which were load tested under uniaxial compression and then geometrically analysed. The remaining 50 samples were not load tested and were only geometrically analysed.

Trends found within the geometric and mechanical data are introduced, analysed, and explained.

Ultimately, two equations were developed from a regression model, which enable a prediction of Energy and Force. These equations were dependent upon two dimensionless parameters; compaction ratio and aspect ratio.

Furthermore, the limitations of the methodology, conclusions, and future direction of research are also discussed.

3| LIST OF FIGURES

Figure 1- Radial Density.....	14
Figure 2- Probability Distribution of ridge length, Blair and Kudrolli (left)	15
Figure 3- Probability Distribution of ridge length, Deboeuf et al. (right)	15
Figure 4- Specimen Positioning Apparatus.....	23
Figure 5- Test Setup	24
Figure 6- Unprocessed 3D Scan	25
Figure 7- Erased Edges.....	25
Figure 8- Global Registration	26
Figure 9- Fast Fusion.....	26
Figure 10- Mesh Simplification	27
Figure 11- Smoothing	27
Figure 12- Unattached Mesh Faces.....	28
Figure 13- Sheet Size, Initial Ball Size, and Ball Size.....	32
Figure 14- Sample Elevation Map (left)	33
Figure 15- Sample Ridge Network (right).....	33
Figure 16- GIMP processed image (left)	33
Figure 17- Grasshopper Analysis (right)	33
Figure 18- Force vs. Displacement. Upper and lower limits are shown for visual clarity. For full, refer to 11.4.1	34
Figure 19- Force vs. Compaction ratio. Upper and lower limits are shown for visual clarity. For full, refer to 11.4.2.....	34
Figure 20- Energy Histogram	35
Figure 21- Total Ridge Length Histogram from 3D scanning method	35
Figure 22- Ridge Length Distribution from Edge Detection Method.....	36
Figure 23- Platelet Area Histogram.....	36
Figure 24- Platelet Perimeter Histogram	37
Figure 25- Adjacency Histogram.....	37
Figure 26- Mean Area vs. Aspect Ratio.....	38
Figure 27- Median Area vs. Aspect Ratio.....	38

Figure 28- Andresen's Ridge Network Trace.....	40
Figure 29- log Perimeter (left).....	42
Figure 30- log-log Perimeter (right)	42
Figure 31- Area Probability Plot for uncompacted samples	44
Figure 32- Final Force vs. Total Ridge Length.....	45
Figure 33- Energy Relationship.....	50
Figure 34- 3D analysis	54

4| LIST OF TABLES

Table 1- Sample Groups	32
Table 2- Terminology	32
Table 3- Intragroup ANOVA p-values.....	39
Table 4- Explanation of Perimeter to Ridge Length Proportionality.....	42
Table 5- Balankin's model for Mean Ridge Length.....	44
Table 6-Intergroup ANOVA p-values.....	47
Table 7- Generalised Linear Model- Total Energy.....	48
Table 8- Generalised Linear Model- Maximum Force	48
Table 9- Reduced Generalised Linear Model- logarithm of Total Energy	49
Table 10- Reduced Generalised Linear Model- Logarithm of Maximum Force.....	50

5| INTRODUCTION

An Empirical Analysis of the Salient Geometric Properties of Crumpled Paper Balls in Compression is a project that attempts to establish relationships between readily identifiable geometric properties of crumpled sheets and their mechanical performance.

This study was conducted by careful geometric analysis of unfolded crumpled paper and relating observed properties to force-displacement data obtained for each specimen.

Within the last decade, there has been increased interest in the mechanics of the seemingly mundane act of scrunching up a piece of paper, which one would naturally assume to be unrelated to engineering.

Mundane as it may be, the mathematics and mechanics of that simple act are quite complex, which has led to many different approaches to the task of understanding what happens inside a crumpled ball of paper. The complexity of this field lies in the stochastic nature of the crumpling process; very minor changes in conditions under which crumples are formed can result in drastically different outcomes. Furthermore, additional complexity arises from substantially varying material behaviours under crumpling, as well as very different methods of crumpling.

Intriguing as such a puzzle may be, the engineering interest lies within the phenomenon that crumpled balls of paper have remarkably high strength and excellent energy absorption properties for their quite minimal density.

At this stage of the research, the end goal of designing a useful way of structurally utilising crumpled thin sheets seems quite far in the distance. This is due to the fact that the behaviour cannot yet be accurately described by a set of equations that relate measurable or designable geometry to strength, in a form such as Force = Crumple Factor x Material Stress x Area.

It is envisaged that crumpled paper may be able to form lightweight deployable structures for purposes such as temporary disaster relief and impact absorption.

Such structures would likely use discarded paper, as a means by which to reduce waste. As such, it is appropriate that the analyses take place upon hand-crumpled samples, as opposed to machine prepared samples.

Nonetheless, the research conducted thus far has attempted to break the problem down into a series of research areas, many of which are highly specific. These fall into the rough categories of Geometry and Mechanical Properties, both of which are further decomposed into analytical and empirical studies.

Naturally, there are some crossovers between investigations into these categories with varying degrees of agreement between results.

Presently, crumpling tends to be characterised by Plate and Beam mechanics, Fractal Dimensions, and Energy modelling. There is a significant depth of research into each of these fields, but there is a distinct lack of connection between fields.

Thus, the research interest of this Thesis Project is in relating the macroscale properties of force and displacement to microscale geometric properties in a manner that may enable a prediction of mechanical performance based on geometry and vice versa.

6| LITERATURE REVIEW

The field of crumpled structures presently has a diverse range of approaches and theories that attempt to understand the phenomenon of crumpling. Presently, there is much discussion about the relationships of measurable geometric properties to mechanical performance. Naturally, there is a significant amount of disagreement on a range of aspects from geometric modelling to energy scaling.

Familiar theories and methods may not have the capacity to describe the phenomenon of crumpling in its entirety, but there seems to be a significant lack in connection between geometric properties and performance. Potentially, part of the difficulty in describing crumpling behaviour may be that engineers and researchers are thinking about the problem in the wrong way. In much the same way that neural pathways through the brain should be thought of in spherical coordinates, as opposed to traditionally unravelling them, a similar change of perspective may be necessary to understand crumpling.

6.1| GEOMETRY

6.1.1| EMPIRICAL

Fundamentally, studying the geometry of a crumpled ball involves dissecting a crumpled ball into its constituent substructures, with properties that vary at different scales.

On a microscale level, such substructures include d-cones and individual fold lines. A mesoscale level considers the connectedness of said microstructures, as well as the facets circumscribed by them. Finally, a macroscale level considers patterns that arise in the fold networks, such as stacking, density, and curvature. It is useful to break the geometry into these hierarchies as it limits the number of parameters that can affect the particular characteristic being studied. That is, each hierarchy is a result of the one below it, but not of the one above it.

Methods to characterise the internal geometry of crumpled structures are often destructive, but there are non-destructive methods of determining the internal geometries, such as x-ray tomography.

6.1.1.1/X-ray tomography

This technique is used by several researchers (Lin et al. 2009; Cambou & Menon 2011; Bai et al. 2010; Bouaziz et al. 2013) to scan aluminium foils, as x-rays pass through paper unaffected, thereby preventing the imaging of paper and other materials that do not interact with x-rays.

The x-ray scans enabled the authors to determine the degree of anisotropy by the "Mean Intercept Length" method. This method generates a random point cloud within a 3D space, and for each point, many radial vectors of the same length are drawn. The mean intercept length of each vector is its length divided by the number of collisions between the vector and a surface of the object. For each vector, a Mean Intercept Vector is created, which is the direction of the initial vector multiplied by its Mean Intercept Length. From all the vectors ascribed to the point cloud, a 3x3 covariance matrix is calculated and its eigenvalues found. The degree of anisotropy is the largest eigenvalue divided by the smallest eigenvalue. Bouaziz et al. arrived at a value of 1.4, which the authors suggest is reasonable basis to assume that crumpling is approximately isotropic, due to its closeness to unity.

This is an important result as it implies that the orientation of specimens should not affect the measurement of mechanical properties significantly.

6.1.1.2/Geometric Properties

Cambou & Menon's paper makes significant steps towards the characterisation of crumpled balls with simple geometric analyses, some of which are easily replicated.

The authors introduced a number of simple parameters by which one can start to build a numerical model of the internal structure.

The first parameter introduced was $\frac{r}{r_0}$, as a measure of how crumpled from its original dimension, r_0 , a thin sheet was.

Their paper considered the macroscale properties of mass distribution, surface orientation, curvature, and the layering of sheets, from which they found a number of interesting results. Firstly, it was found that the void distribution by radius was quite heterogeneous, as there was quite a large amount of variation in mass distribution by radius across each sample. Overall, there was a trend of a slight increase to a maximum density at $r/r_0=0.8$, followed by a sharp decrease (Figure 1). This is in contrast to assumptions used by Alexander S. Balakin et al. 2013 and Bevilacqua 2004.

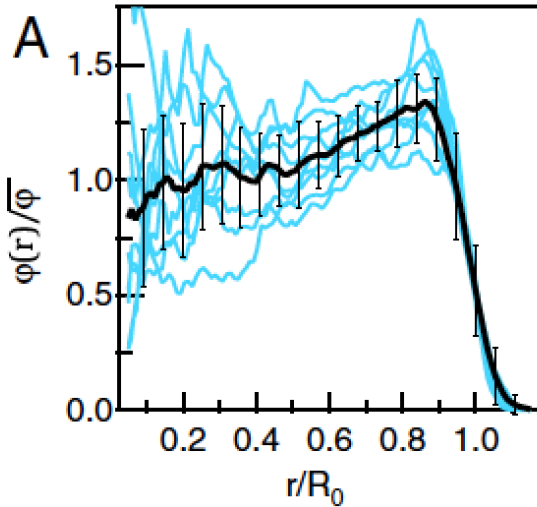


Figure 1- Radial Density

Furthermore, the authors found that the surface normals were nearly isotropically distributed, which is surprising, given that symmetry would not be expected from a process such as crumpling. This result is in concert with findings by researchers modelling energy as the "average energy along a ridge" (Alexander S. Balakin et al. 2013; Tallinen et al. 2009; DiDonna 2002), as isotropic surface orientation could suggest likewise about ridge distributions.

The approach to quantifying curvature was not direct, as ellipsoids were fitted to connected patches of the sheet. Smaller ellipsoids correspond to smaller radii of curvature, and it was found that curvatures were uniformly distributed. This may be explained by the observation of a limiting value of curvature, approximately 10x thickness, beyond which the crumpling process creates new folds, rather than buckling existing ones.

The fourth geometric characteristic, stacking, was quantified by the probability of 3D surface normals being parallel at a given radius. It was found that this probability increases approximately linearly with radius, regardless of the number of sheets in a stack. This implies that stacking is initiated from the outside and works inwards.

Though Cambou and Menon's work is thorough and describes crumpled sheets by familiar properties, their data size of nine samples is far too small to draw any reliable conclusions, especially given the large variance per sample, as illustrated in Figure 1.

6.1.1.3/ Facet Analysis

Another common technique amongst the papers was to carefully unfurl the crumpled paper and perform analyses on the flat sheet (Deboeuf et al. 2013; Bevilacqua 2004), sometimes aided by the use of laser microtomography (Andresen et al. 2007; Blair & Kudrolli 2005).

Deboeuf et al.'s paper compared the behaviour of crumpling to that of folding numerous times, both analytically and empirically. The authors rationalise that the two can be related, as both have similar power law relationships regarding force and compaction ratio.

Deboeuf et al.'s most interesting conclusion is based upon the well-fitted nature of a lognormal to the probability distribution of ridge length, based upon a χ^2 test, a result similarly found by Lin et al. 2009 and Balakin et al. 2007, but contrasted by Tallinen et al. 2009. Deboeuf et al. claim that such a distribution is indicative of a hierarchical process. This means that in order for particular crumpled substructures to be formed, a certain sequence of folds must occur.

Similarly, Blair & Kudrolli plot the probability distribution of ridge length, but their results are drastically different to Deboeuf et al.'s. It can be seen in Figure 2 that there is a decrease in probability from $10^{-0.9}$ to $10^{-1.5}$ between lengths 10^0 and 10^1 . However, in Figure 3, there is an increase of probability from 10^{-2} to $10^{-1.2}$ between lengths 10^0 and $10^{0.7}$, followed by a decrease in probability to $10^{-1.7}$ between lengths $10^{0.7}$ and 10^1 .

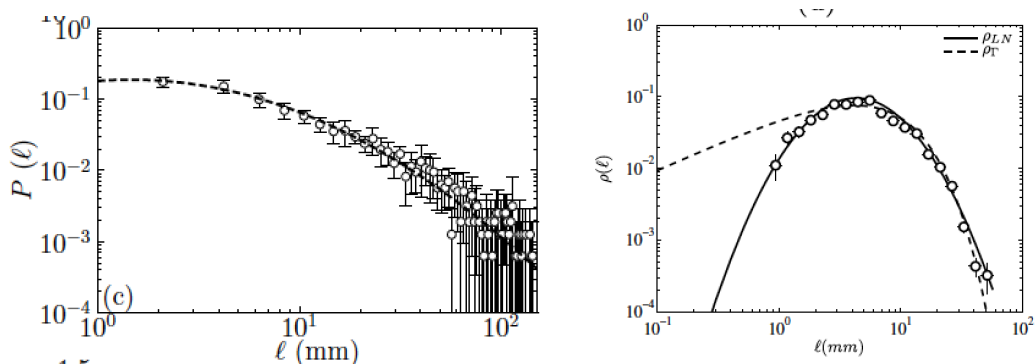


Figure 2- Probability Distribution of ridge length, Blair and Kudrolli (left)
 Figure 3- Probability Distribution of ridge length, Deboeuf et al. (right)

Upon examination of the procedures used, the disparity becomes obvious. Blair & Kudrolli scanned an entire crumpled piece of paper, whereas Deboeuf et al. used a hot wire to dissect the ball and plotted a probability distribution of the perimeters of the cut segments. They mistakenly equated the perimeter of the cut segments to ridge lengths.

The broad range of techniques in the aforementioned papers indicates that methods to understand the geometry and mechanics of crumpling are still in their infancy. Consequently, little can be safely assumed due to the complexity and relative lack of understanding of the crumpling phenomenon.

6.1.2| ANALYTICAL

An analytical approach to the geometry of crumpled structures goes hand-in-hand with an energy analysis. Typically, geometric analyses are limited to a single crumpled sub-structure and are very assumption dependent. Such assumptions include that the sheet is globally smooth, neglect of "higher order terms", the radii of curvature of plates are much greater than their thicknesses, and the orders of magnitude of bending and stretching energies are similar.

6.1.2.1/ Gaussian Curvature and Energy

Intrinsic to many of these analyses is the concept of Gaussian curvature, which is the product of the two principal curvatures of a surface, that is:

$$\kappa_{gauss} = \frac{\delta^2 f(x,y)}{\delta x^2} \cdot \frac{\delta^2 f(x,y)}{\delta y^2}$$

What Gaussian curvature implies is that only objects with identical Gaussian curvature can be mapped to each other with no distortion. This is the reason why the map of the globe cannot be translated to a flat sheet, as spheres have Gaussian curvature R^{-2} whilst flat, planar sheets have zero Gaussian curvature.

The most general analysis of the geometry simply enforces that a smooth developable surface (a sheet with zero Gaussian curvature) is constrained to pass through a non-planar curve in \mathbb{R}^3 (the boundary curve of the sheet in its deformed state). It also requires that the global deformation energy be minimised in order to achieve a stable configuration that satisfies the previous requirements.(Ben Amar & Pomeau 1997) This allows the authors to arrive at the conclusion that external force cannot appear as a scaling factor, contrary to a paper written by Landau and Lifchitz 1990.

Landau and Lifchitz arrive at a lengthy two-part equation that is a condition that a crumpled geometry must meet, but is by no means a functional descriptor of such geometry.

The main limitations of the aforementioned equation are that it does not specifically describe the minute behaviours on an individual ridge-by-ridge basis, and it requires that the surface be considered globally smooth.

Nonetheless, the authors arrive at an inner and outer solution for the stress near a D-cone.

$$\sigma_{\text{outer}} \approx \frac{Eh^2}{r^2}, \quad \sigma_{\text{inner}} \approx Eg_0^2, \text{ where } g_0 \text{ is a dimensionless measure of the angular opening of the d-cone}$$

The properties of such D-cones are further investigated by Efrati et al, who arrive at the result that the geometry of the disc can be characterised by a single parameter, ∂/ε^2 . This parameter relates ∂ , the angle of the wedge removed from a disc to ε , the degree of confinement. The authors also produce an energy equation that is the integral of the stress and curvature about a closed curve. This form is consistent with that presented by Aharoni & Sharon 2010.

6.1.2.2/ Fractal Dimension

Generally defined, fractal dimension is a measure of how detail changes depending upon the scale at which it is measured. In the case of crumpling, it refers to how sheet size affects compaction at a given force and is approximately of the form $R \sim L^{2/D}$, where R is the size of the crumpled ball and L is the linear dimension of the original sheet. The Fractal Dimension, D is bounded by limits 2 and 3, with lower values indicating it is close to planar (Tallinen et al. 2009).

Often, Fractal Dimension is calculated from an exponential scaling relationship with force (F):

$$D = \frac{2}{1+2\beta-\alpha}, \text{ where } \alpha \text{ and } \beta \text{ are defined by} \quad (\text{Lin et al. 2009})$$

$$\frac{R}{R_0} \propto \left(\frac{ER_0^2}{B}\right)^\beta \left(\frac{B}{FR_0}\right)^\alpha, \text{ where } E - \text{Young's Modulus, } B - \text{bending rigidity}$$

$$D = 2 + \frac{2(1-\beta)}{\beta + (2-\beta)\alpha}, \text{ where } \alpha \text{ and } \beta \text{ are defined by}$$

$$\bar{l} \propto L \left(\frac{L}{R}\right)^{-\alpha}, \text{ where } \bar{l} \text{ is average ridge length} \quad (\text{Balakin et al. 2013; Tallinen et al. 2009})$$

$$N_R \propto \left(\frac{L}{R}\right)^{2\alpha}, \text{ where } N_R \text{ is total number of ridges}$$

$$F \propto L^{2\mu/D} R^{-\mu}, \text{ where } \mu = 1 + (2 - \beta)\alpha$$

Lin et al. briefly proposes that Fractal Dimension is material dependent, suggesting that Fractal Dimension may not be an appropriate measure by which to compare samples, which is contrasted by Balakin et al. They propose that Fractal Dimension is a characteristic number that describes all crumpled structures, which is referenced and refuted by Lin et al. Balakin et al. draw this conclusion from their experiments and simulation, which is flawed considering that experimentally they determined $D=2.5 \pm 0.1$, whilst from simulation $D=2.3 \pm 0.1$. These two

results are outside of the confidence interval of each other, suggesting that they are measuring two entirely different properties.

Furthermore, Cambou & Menon 2011 suggest that Fractal Dimension is not a particularly useful dimension in describing the internal structure, as the Fractal Dimension is generally calculated as an average over the entire ball.

The aforementioned analytic equations describe the geometry without any consideration of the process that forms the geometries, which Bevilacqua's investigation attempts to establish. He assumed that the crumple process is random, homogeneous, has negligible second order effects, and is frictionless.

According to Cambou & Menon, the assumption of homogeneity is not substantiated, and friction has been shown to significantly impact crumpling behaviour as it enables ridges to interlock. (Quach 2014; Cambou & Menon 2011; Alexander S Balakin et al. 2013). Friction was similarly neglected by other authors (Tallinen et al. 2009; Bouaziz et al. 2013; Peraza-Hernandez et al. 2014; Efrati et al. 2014).

Nonetheless, Bevilacqua introduces some relationships, which are derived from scaling relationships based upon Fractal Dimension:

$E = Kt^2(\sum I_R)\bar{\theta}$, which states that the total energy is a function of the ridge stiffness, thickness, total ridge length, and average relative rotation

This can be simplified down to $\frac{E}{S_0} = K\alpha t^2 \frac{\bar{\theta}}{\delta_R}$ by $\sum I_R = \alpha \frac{S_0}{\delta_R}$, where α is a parameter dependent on tile geometry and δ_R is the average ridge length

This presents the conclusion that energy density is proportional to relative rotation (dihedral angle) and inversely proportional to average ridge length.

A key assumption in the above equation is "self-similarity", which means that one part of the object is similar to its entirety. Such a condition is not characterised, but is substantiated by Balakin et al. 2007, who conclude that self-similarity is a property of crumpled thin sheets.

6.2| MECHANICAL PROPERTIES

6.2.1| EMPIRICAL

Empirical investigations into mechanical properties are not particularly informative unless some form of geometric analysis complements them. This enables correlations to be drawn between performance characteristics to geometric properties.

Comparisons have been made between the behaviour of a crumpled aluminium ball and the behaviour of foams and entangle fibrous materials (Bouaziz et al. 2013). The exact purpose of these comparisons was not explained, but possibly inferred that one may characterise crumpled balls by an equivalent foam-entangled fibre combination.

As to the correlations themselves, the authors concluded that like foams, crumpled paper balls exhibited clear plasticity and a power law relation between relative density, relative Elastic Modulus, and relative yield strength:

$$\frac{E_0}{E_s} \propto \left(\frac{\rho_0}{\rho_s}\right)^n \quad \text{and} \quad \frac{\sigma_0}{\sigma_s} \propto \left(\frac{\rho_0}{\rho_s}\right)^m$$

Unlike foams, and more like entangled fibrous materials, the crumpled aluminium balls exhibited very similar strain hardening effects. Unfortunately, these behaviours were not compared to other material samples, thereby limiting the applicability of their results to only materials with similar stiffness and plasticity to aluminium. Particularly, the strain hardening observation was not reported on in any other literature other than in reference to paper's material properties.

It was more common for papers to discuss strain relaxation of paper balls. (Aharoni & Sharon 2010; Peraza-Hernandez et al. 2014; Alexander S Balakin et al. 2013) This phenomenon concerns how the sheets will release or redistribute some of the elastic energy stored in the ridges over time.

6.2.2| ANALYTICAL

6.2.2.1/ Beam Theory

The most basic model is a simply-supported beam model. (Baillie & Johnston 1991; Baillie & Johnston 1992) A developable surface is broken down into discrete triangulations, suitable for numerical modelling. The particular model type was a "dynamical mesh", which describes how for a fixed rule in a given state, there is only one future outcome. This concept attempts to describe the effect that minute perturbations have upon the global result, as each crumple is unique. This implies that each crumple is a result of the minute differences in sheet geometry, crumple process, material properties, and a plethora of other factors, many of which might be as yet unknown. A shortcoming of this method is that it neglects the effects of bending within the facets and the storing of energy within ridges and vertices. This is suggested by the authors in reference to higher order effects in a "transitional buckling region", where there is

a change in dominant regime from the formation of discrete ridges to the formation of layered structures.

6.2.2.2/ Network Theory

A parallel model is that of Network Theory (Andresen et al. 2007), whose investigation, although empirical, utilised concepts of clustering and probability distributions.

Networks consist of nodes and links, which, in the context of crumpling are the vertices and fold lines, respectively. A network model such as this examines the global effect of actions that occur on the local scale, and vice versa.

This served the purpose of determining the extent to which each fold or node affected its neighbours. Some measures that have been used are node degree and clustering coefficients. The former describes the number of links at a node and the latter refers to the connectedness of nodes. These characteristics are theorised to describe how robust or sensitive the crumpled network is to being broken or altered.

6.2.2.3/ Plate Theory

A more common starting point in most analyses is that of Plate Theory, with particular reference to the von Kármán equations, from which bending energy is derived. (Ben Amar & Pomeau 1997; Aharoni & Sharon 2010; Lobkovsky & Witten 1996)

The justification of this method is that a crumpled sheet is composed of planar facets connected by fold lines. These can be thought of as elastic plates connected by hinges with finite rotational stiffness.

Various modifications are often allowed for, as seen previously in reference to Amar & Pomeau's allowance for extensional energy due to generation of finite Gaussian curvature within D-Cone regions.

Conceptually, this particular model may be the easiest to model in basic analysis packages like Grasshopper for Rhino, using plugins such as Lunchbox and Kangaroo. The facets of a crumpled sheet can be modelled according to an appropriate probability distribution, be it power law (Tallinen et al. 2009; Deboef et al. 2013), lognormal (Andresen et al. 2007), or otherwise. Each facet's ridges can then be assigned appropriate rotational and extensional stiffnesses, depending upon the distribution chosen.

6.2.2.4/ Buckling Analysis

Plate theory can then be extended to a buckling analysis of thin shells, whereby energies can be compared at different stages of the buckling process. (Didonna 2006) Both theoretical and simulation approaches were taken with some mild discrepancies. These were reasonably explained and quantified by certain inadequacies in the theory and simulation, allowing for an arrival at relatively similar results.

Didonna compared the behaviour of a ridge during the buckling transition to that of a thin cylinder, both of which exhibit identical bifurcation.

Specifically, it is shown that the rate at which the stiffness of the ridge approaches zero, with increasing stress, is in the same order of magnitude as that of a thin cylinder.

Didonna presents a useful energy scaling relation, based upon the von Kármán equations:

$$E \sim \kappa \lambda^{\frac{-1}{3}}, \quad \kappa - \text{dimensionless energy}, \quad \lambda - \text{dimensionless thickness} \sim \frac{1}{12(1-\nu^2)} \frac{h}{X} \quad . \quad \text{Furthermore,}$$

Didonna shows that the elastic energy scaling on ridges at rest is identical to that of those at the buckling transition. However, there is a sharp discontinuity between pre and post-buckled states as there is rapid formation of ridges.

METHODOLOGY

6.3| AIM

In order to characterise and understand the macroscale behaviour of crumpled thin sheets, the effect of microscale and mesoscale properties must first be understood. Macroscale properties refer to the mechanical performance of the crumpled sheets, whilst microscale properties refer to localised geometric properties, such as ridge lengths. Mesoscale properties concern the relationships between microscale properties, such as the connectivity of ridges. There have been a number of properties that have been explored by researchers, some of which are in conflict with each other's results.

These properties include ridge length, facet size, node degree, fractal dimension, and compaction ratio.

The basic premise of crumpling is that the sheet is irreversibly deformed, during which energy is absorbed, creating a pattern of intersecting ridges, which indicate areas of high stress concentration.

6.4| HYPOTHESIS

It is the purpose of this thesis project to determine the salient parameters that influence the relationships between and properties within the micro, meso, and macroscales of crumpled paper balls, such that a prediction of the mechanical behaviour can be made based upon the geometric properties.

6.5| APPROACH

An empirical method was adopted to enable the determination of relevant parameters such that predictions of mechanical behaviour may be made.

6.6| SAMPLE PREPARATION

6.6.1| MATERIALS

The samples were made from ordinary copy paper, so as to keep with the vision that ordinary and recycled papers may eventually be used to create a structure. Once crumpled, the samples were allowed to undergo stress relaxation for a minimum of 10 days so that any elastic energy trapped within the ridges may be allowed to dissipate.

6.6.2| SIZE

It was uncertain whether the proportions of a flat sheet would have significant impact upon the mechanical performance of the crumpled paper ball. It was decided to use square sheets of paper (210x210mm), cut down from a standard A4 sheet (210x297mm), so that the characteristic length of the sheet was any of the side lengths.

6.6.3| SAMPLE SIZE

300 samples were used to increase the precision of the data correlation.

6.6.4| SPECIMEN POSITIONING APPARATUS

To hold the samples in place, a piece of timber with a dimple in it was used to prevent the samples from rolling when loaded. The thickness of the timber and depth of the dimple was recorded, as this would affect the final ball size.

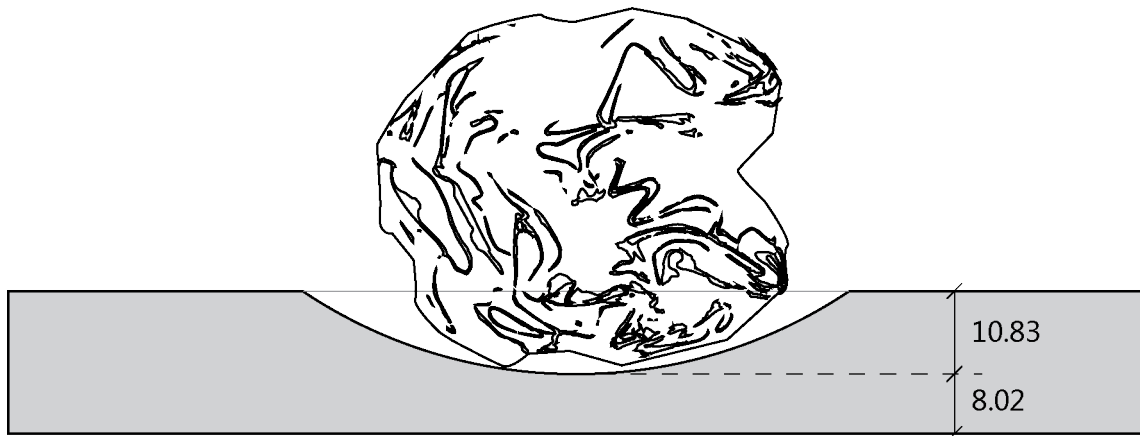


Figure 4- Specimen Positioning Apparatus

6.6.5| LOAD TEST

Each sample was load tested on an MTS Criterion Series 40 Load Cell until it reached a predetermined final size, at which point the test was stopped by means of a limit switch. This limit switch displaced by a constant 1.74mm before activating, making the final sample sizes slightly smaller than initially determined. The samples were loaded at a rate of 30mm per minute.

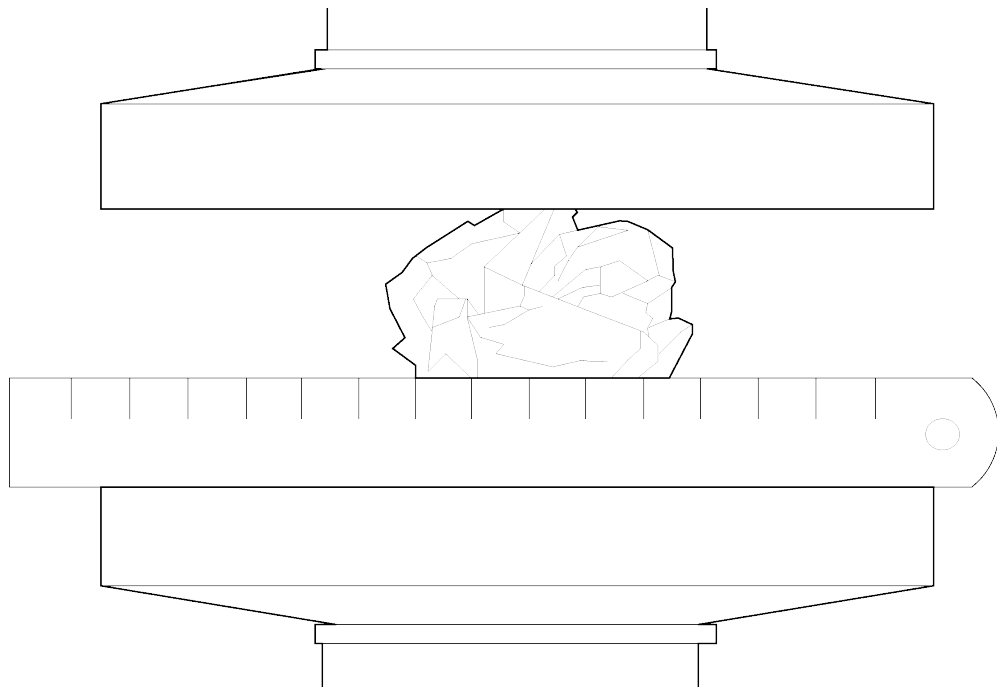


Figure 5- Test Setup

6.6.6| 3D SCANNING

The crumpled ball was then unfolded and scanned using an Artec3D Spider 3D scanning camera, in order to obtain a digital model of the unfolded geometry, so that the measurement of ridge lengths and other geometric properties could be conducted.

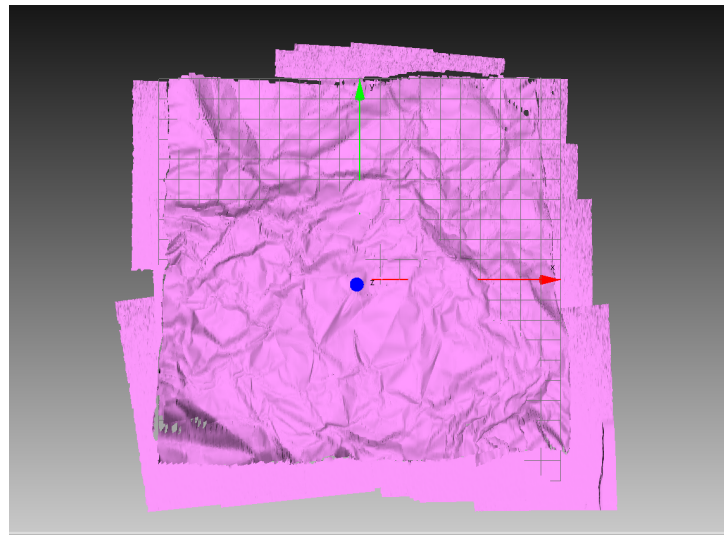


Figure 6- Unprocessed 3D Scan

The scans required post processing in Artec3D Studio 10 Pro, where a number of built in algorithms were applied:

1. Any mesh faces that "hung" off the edge of the scan were removed manually.

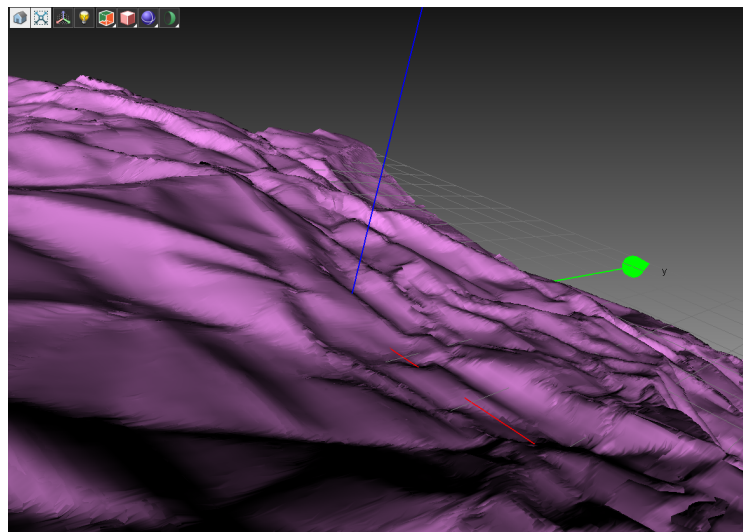


Figure 7- Erased Edges

2. The Fine registration process was applied. This accurately aligns each frame that was captured by the camera so that post-processing may commence. The term "fine" does not refer to any threshold value, but rather that the alignment and processing takes place on a frame-by-frame basis.

3. A Global registration was applied. This optimises the data storage and relative position of all frames within a single coordinate system.

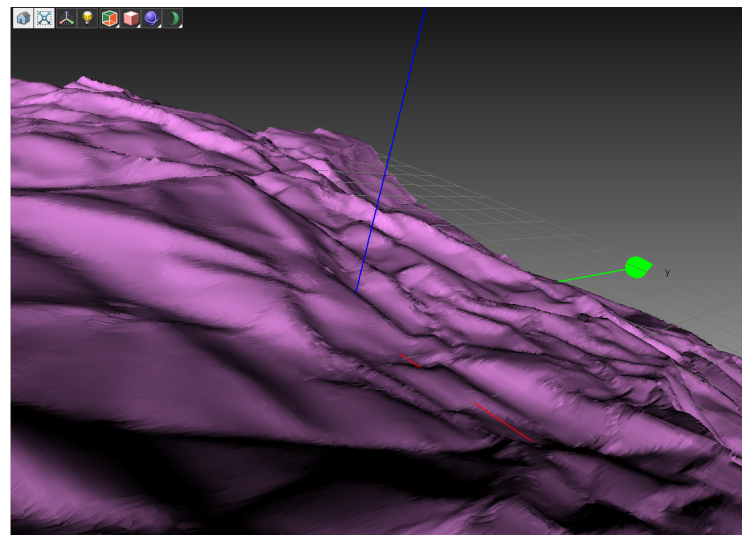


Figure 8- Global Registration

4. Fast Fusion was applied. This causes all the frames to become a single polygonal 3D model. There are a number of fusion settings, but for the sake of time, Fast Fusion was chosen, which is the least memory consumptive algorithm and is best suited to working with large data sets.

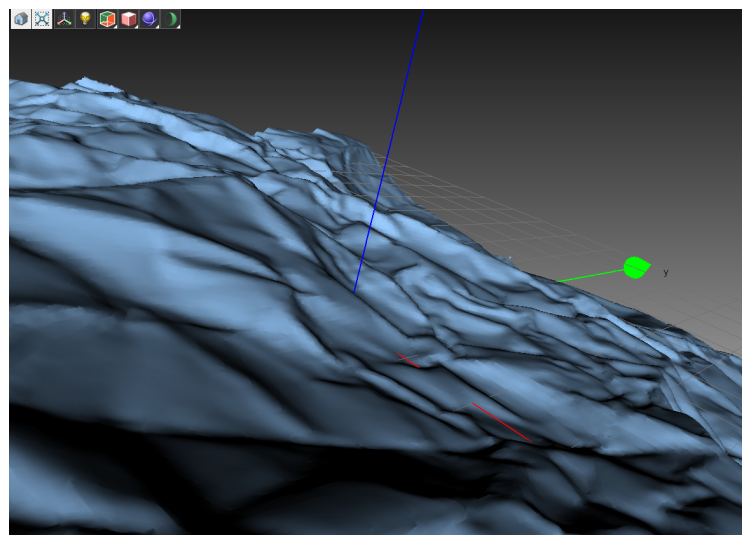


Figure 9- Fast Fusion

5. A Hole filling algorithm was applied to correct for mesh faces that may have been lost during the previous algorithms.

6. A Mesh Simplification algorithm was applied to reduce the file size and eliminate noise inherent to a Fast Fusion. A maximum deviation of 1% was set, which allows for a maximal reduction in mesh faces, and hence file size, whilst maintaining an accurate representation of the mesh scan. This enables the file to be readily handled by computers not specifically optimised for 3-D modelling and analysis.

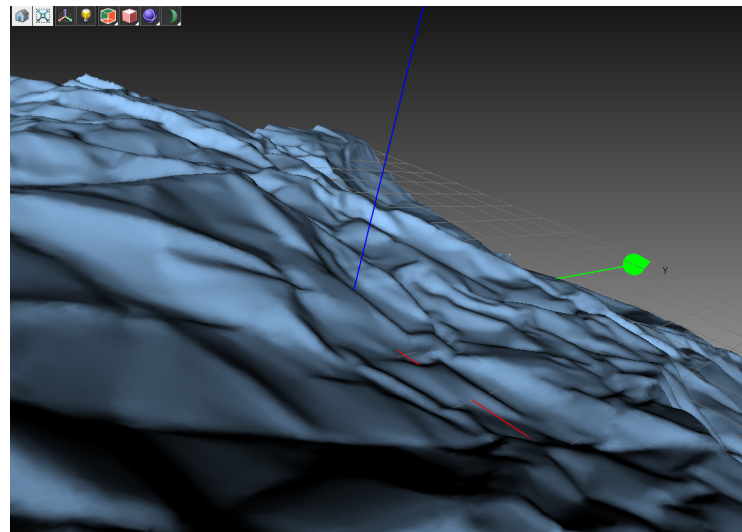


Figure 10- Mesh Simplification

7. A Smoothing algorithm was applied to further reduce noise that may cause a false positive measurement to occur.

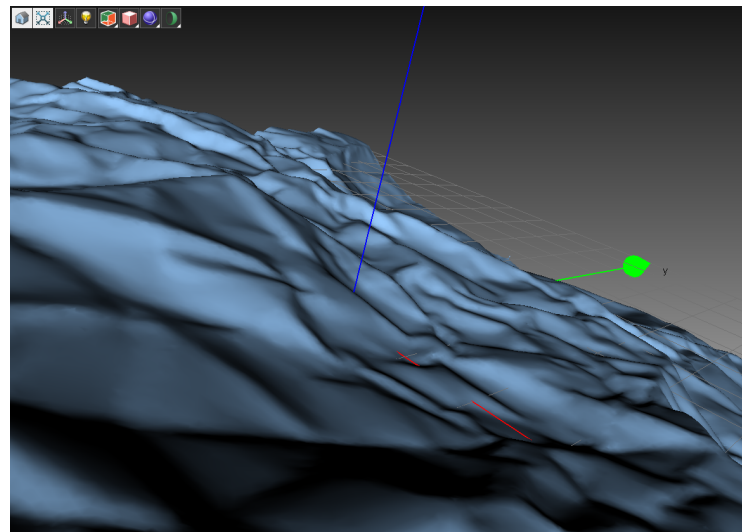


Figure 11- Smoothing

8. Each sample was exported as a 3D mesh to a Wavefront Object File (.obj).

6.6.7| 3D MODEL ANALYSIS

Each sample was first imported into Rhinoceros and further processed to remove unattached meshes. It is important to not have unattached meshes, as it could cause unpredictable data structures to occur when imported into the Grasshopper for Rhino plugin. Illustrated below in Figure 12 are examples of unattached mesh faces.

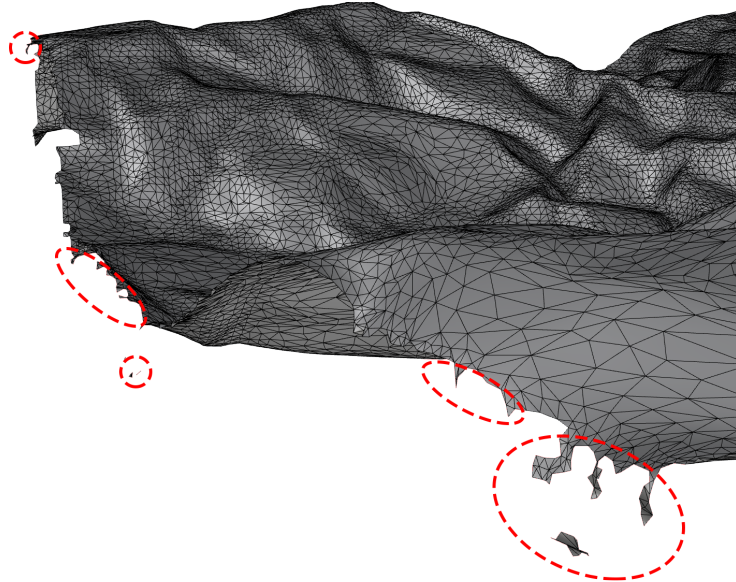


Figure 12- Unattached Mesh Faces

Originally, it was envisaged that Grasshopper would be able to convert the 3D mesh into a wireframe by means of the various curvature-processing tools contained within Grasshopper and its many toolboxes. Unfortunately, like Andresen et al and other researchers before us, automating the process to a level suitable for use on large sample groups proved to be out of our reach.

Instead, Grasshopper was used to analyse the heights of each sample at a regular 0.1mm grid in the x-y plane, which was then converted into a greyscale image of varying size, but used the constant scale of 1 pixel width = 0.1mm, which is the limit of accuracy of the 3D scanner. Therefore, decreasing the grid spacing will not increase the accuracy, but may introduce some errors as linear interpolation must be used to find points in between measurements.

6.6.8 | IMAGE PROCESSING

Once the images were obtained, they were batch processed in MATLAB's Image Processing Toolbox. Outlined below is a summary, but for the full code, refer to pg57.

1. The vectors to contain the results of the image processing were preallocated. This gives them a defined size, and makes the code run faster as MATLAB does not have to create new matrices and copy the old matrix across whenever a new element needs to be added.
2. For each image and its complement image, the watershed function was applied. The Watershed function in MATLAB's Image Process Toolbox is used in water catchment analysis to divide an elevation image into regions drained by the same rivers. What this translates to in the context of crumpled paper is that it is detecting the mountain folds. Hence, the complement image must be analysed, as the previously undetected valley folds become mountain folds.
3. The two images are added together to create an approximation to the complete ridge network
4. The new image is divided into connected black and white components and assigns each a label. These connected white components approximate facets, but may contain smaller ridges, and as such, the term "facet" is not appropriate. Henceforth, these regions shall be referred to as platelets.
5. The connected black components approximate the complete ridge network. These black components are always 1 pixel wide, therefore, counting number of pixels and applying the scaling factor of 1 pixel = 0.1mm will give the total ridge length.
6. Each platelet was analysed to determine Area, Perimeter, and Adjacency. Adjacency refers to the number of platelets that share a boundary with the platelet under consideration.

Concurrent to this method of investigation, the unfolded samples were scanned using a flatbed scanner at 250 DPI. This method was developed as preliminary investigations into the Watershed function revealed that not all edges were detected, and thus, it was uncertain if an accurate total ridge length could be obtained. The assumptions of these two methods shall be discussed on pg40.

The scanned images were then converted to a binary image in the image-processing program "GIMP" (GNU Image Manipulation Program).

The binary image represented the ridges as white, whilst the areas in between were black. The Neon Detection function (a type of edge detection) with parameters radius=10, amount= 0.3 was found to give the best results, by visual inspection.

The processed images were then imported into Grasshopper for Rhinoceros, and the total area of the white regions was found. To achieve this, the image was broken into a grid and the white areas populated with circles of varying sizes below a maximum diameter of 1.5mm to prevent overlap. The total area of these circles was found and calibrated by tracing one entire ridge network in Rhinoceros. The total length of this network was found, which was used to divide the area sum to give an effective thickness, which can be used to scale the areas of subsequent samples. For the full Grasshopper definition, refer to pg62.

6.6.9| DATA ANALYSIS

Once the geometric data was obtained, the Force-Displacement data taken from the MTS Criterion Load Cell was imported into MATLAB, from which a number of measures may be calculated for each sample:

- Incremental and Final Ball size (mm). This required the input of final ball size, which was accurately known for each sample.
- Maximum Force (N)
- Maximum Displacement (mm)
- Aspect ratio- referred to as r/r_1 , where r refers to the present ball size and r_1 refers to the initial ball size post-hand-crushing
- Compaction ratio- referred to as r/r_0 , where r_0 refers to the sheet size.
- Incremental and Total Energy (J)
- Incremental Stiffness (N/mm)

Initially, frequency distribution plots and x-vs-y plots were created to gain a preliminary understanding of the data. The samples were grouped according to compaction ratio and Analysis of Variance tests (henceforth referred to as ANOVA) were performed on each group to determine if the samples within each group were statistically distinguishable from one another. ANOVA was performed to test the hypothesis that each compaction ratio's geometric characteristics were different from the next. If this is true, then it is reasonable to infer that these geometries were a result of being compacted to differing degrees. If false, however, it cannot be concluded that compaction had a significant effect upon the geometries formed.

Though MATLAB's ANOVA function was apparently able to handle unbalanced data, the data sets were heavily unbalanced (sometimes by over 200%), and it was surmised that this might significantly affect the results. To confirm that the ANOVA test was giving the correct p-value, all samples were interpolated such that their lengths were equal to the longest in the group. The frequency distribution plots and p-values of the balanced and unbalanced data were compared and it was found that the results were identical.

7| RESULTS

7.1| INITIAL REMARKS

Group Name	Final Ball Size (mm)	Contains samples	Colour on Figures
0	Untested	251-300	Magenta
10	11.74	1-50	Blue
15	13.26	148-150, 204-250	Green
20	18.26	51-100	Red
25	23.26	101-147, 201-203	Cyan
30	28.26	151-200	Black

Table 1- Sample Groups

Upon initial investigation of the results, it was noticed that the total ridge lengths, Areas, Perimeters, and Adjacencies of the samples corresponding to the final ball sizes of 25mm and 30mm appeared to be switched. Through the use of Mann-Whitney U-tests, it was determined that the samples had in fact been switched, either during testing or during scanning. It was decided, based upon these results to rename the load-displacement data files such that they matched the order in which the images were scanned. The correct groupings are seen above in Table 1. For the full reasoning and results of the Mann-Whitney tests, refer to pg63.

Throughout this Thesis, the following terminology will be used:

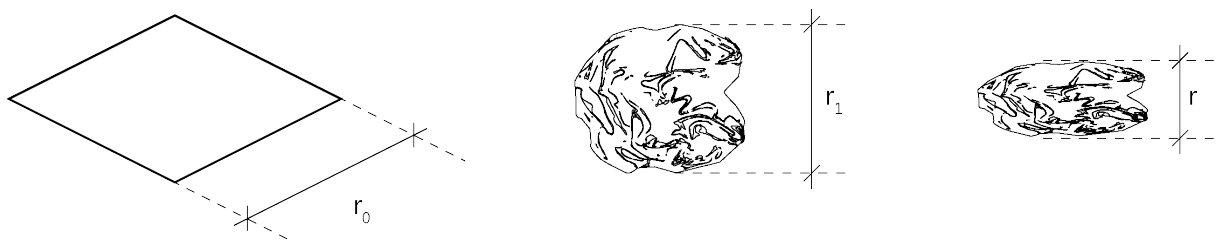


Figure 13- Sheet Size, Initial Ball Size, and Ball Size

r/r_0	Compaction Ratio	r/r_1	Aspect Ratio	t	Thickness
L	Total Ridge Length	l	Ridge Length	\bar{l}	Mean Ridge Length
E	Energy	F	Force		

Table 2- Terminology

7.2| DATA

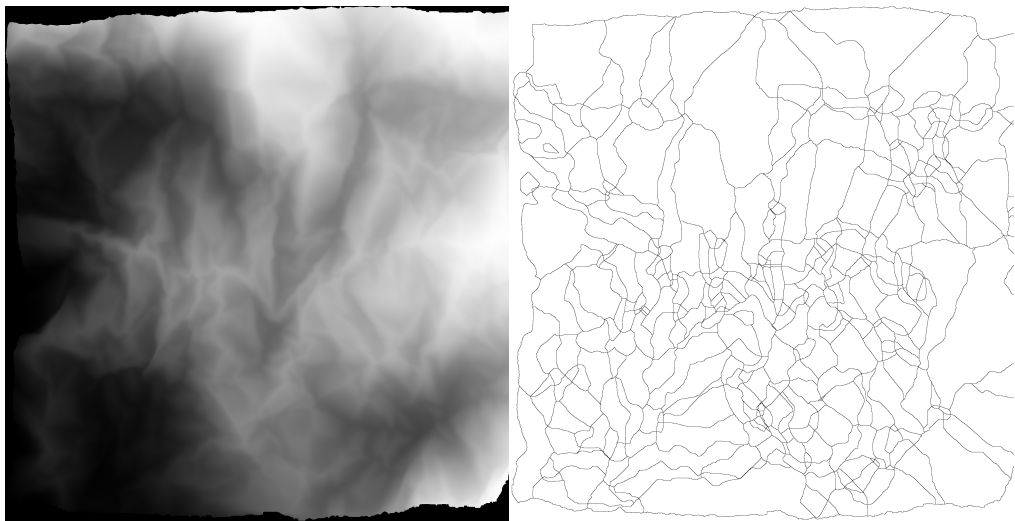


Figure 14- Sample Elevation Map (left)

Figure 15- Sample Ridge Network (right)

The above images were produced through the 3D scanning and image analysis processes for the same sample. Figure 14 is produced by Grasshopper, with each pixel value representing a normalised height of the corresponding (x,y) coordinate. Figure 15 is produced by the MATLAB image processing script. It is a binary image, in which the black lines represent the ridge network and the white spaces are platelets. It can be seen that there are more ridges present in Figure 14 than detected in Figure 15, but we believe that it is a good approximation, as most of the ridges that were visually identified were detected.

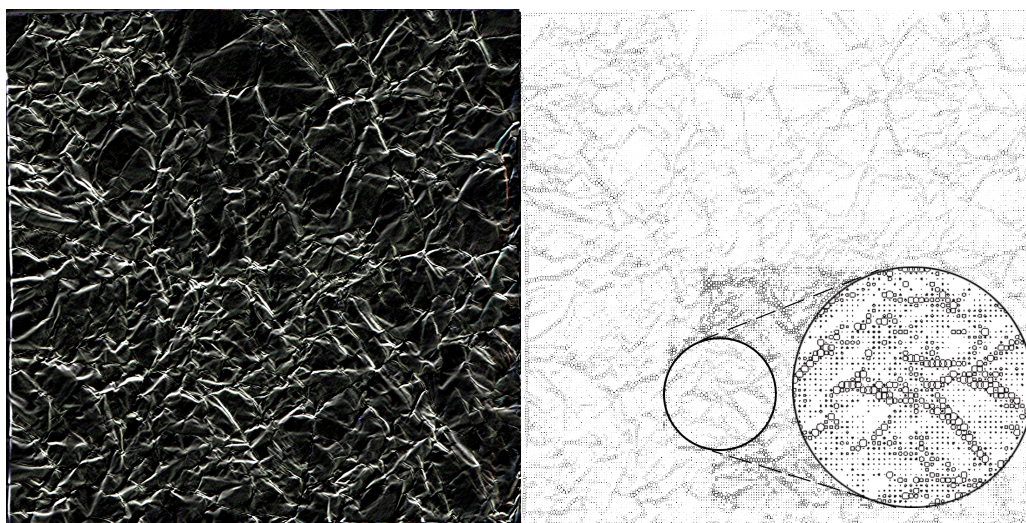


Figure 16- GIMP processed image (left)

Figure 17- Grasshopper Analysis (right)

The above images were produced by the 2D edge detection method for the same samples displayed the 3D scanning method. Figure 16 is a greyscale image produce by GIMP, where the white lines represent ridges. Figure 17 consists of a number of circles, which are used to measure the areas of the ridges.

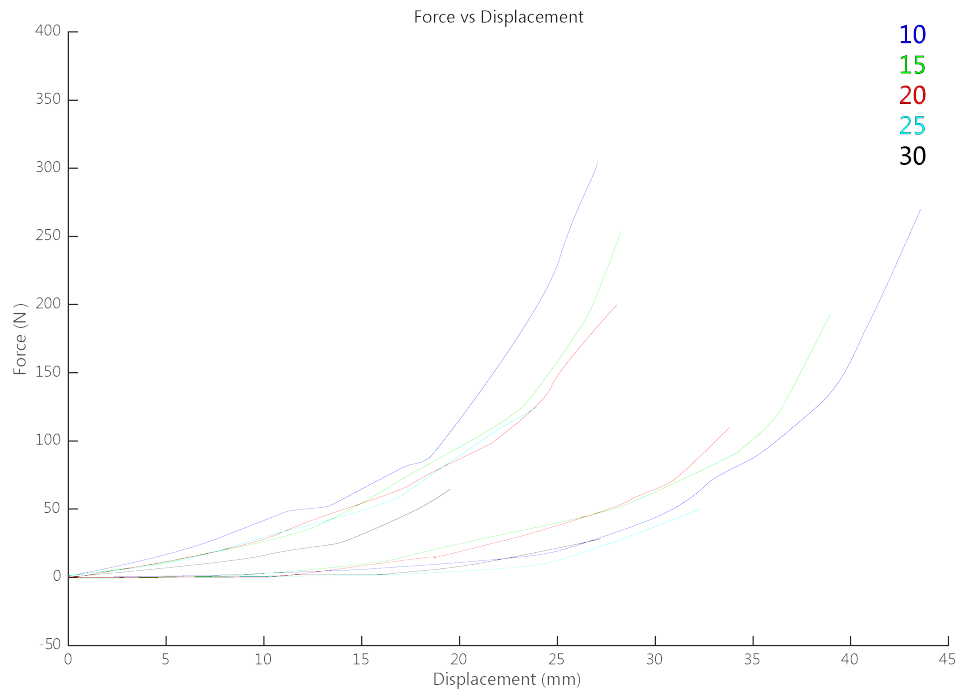


Figure 18- Force vs. Displacement. Upper and lower limits are shown for visual clarity. For full, refer to pg65

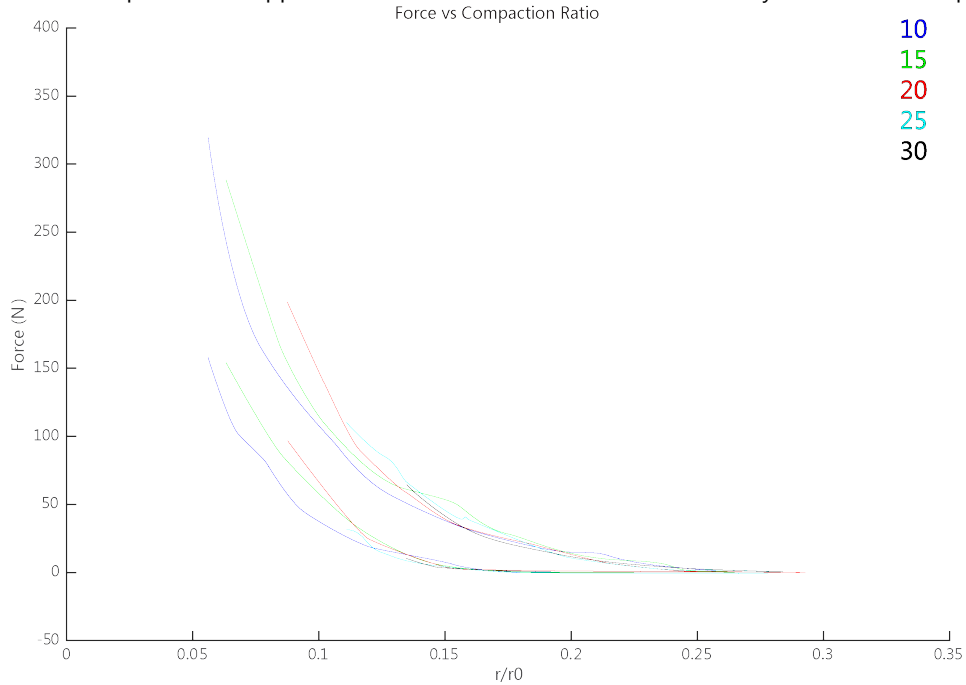


Figure 19- Force vs. Compaction ratio. Upper and lower limits are shown for visual clarity. For full, refer to pg65
The above figures are plots of force against displacement and compaction ratio, respectively.

It is important to note that there are two curves of each colour, which represent the upper and lower bounds of the spread of data for that group. It can be seen that as displacement increases and compaction ratio decreases, the force increases. The relationship between force and displacement will be discussed later.

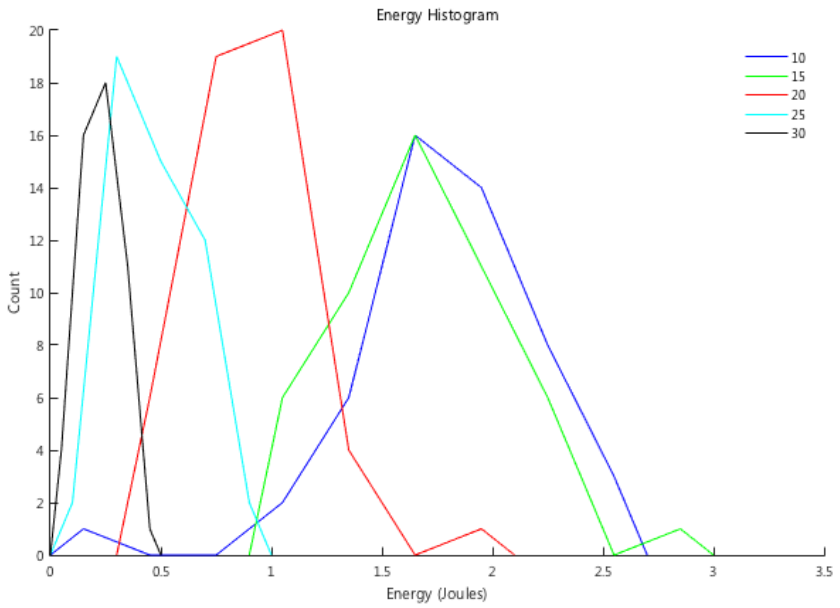


Figure 20- Energy Histogram

The above figure shows that the total energy increases as final ball size decreases. This is expected, as energy increases with force and displacement. It is important to note that the variance of the energy increases as energy increases, and shall be discussed.

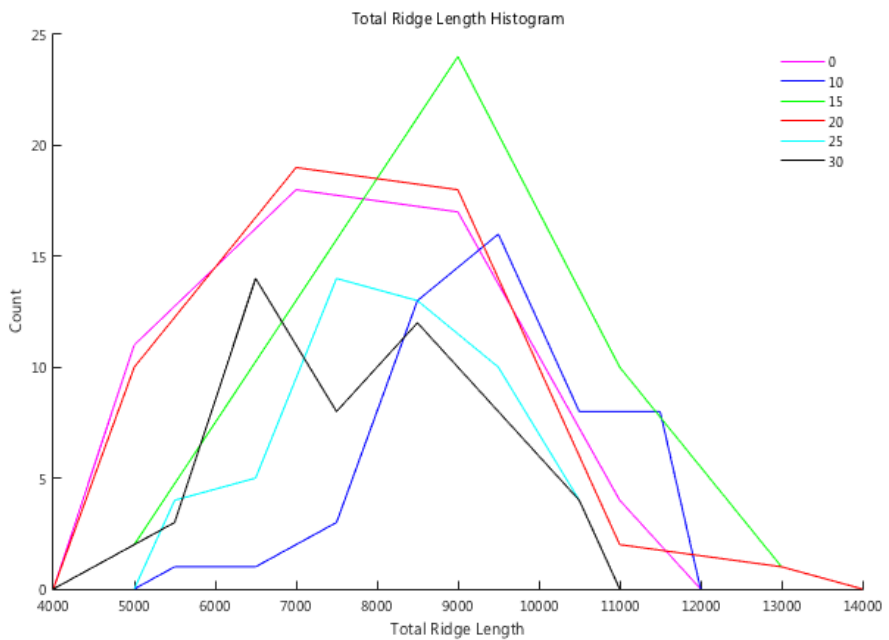


Figure 21- Total Ridge Length Histogram from 3D scanning method

Figure 21 shows the distribution of total ridge lengths. Upon preliminary inspection, clear trends cannot be confirmed. Therefore, ANOVA was conducted to determine if samples are statistically distinct. This was to test the hypothesis whether the total ridge length was significantly different across compaction ratio groupings.

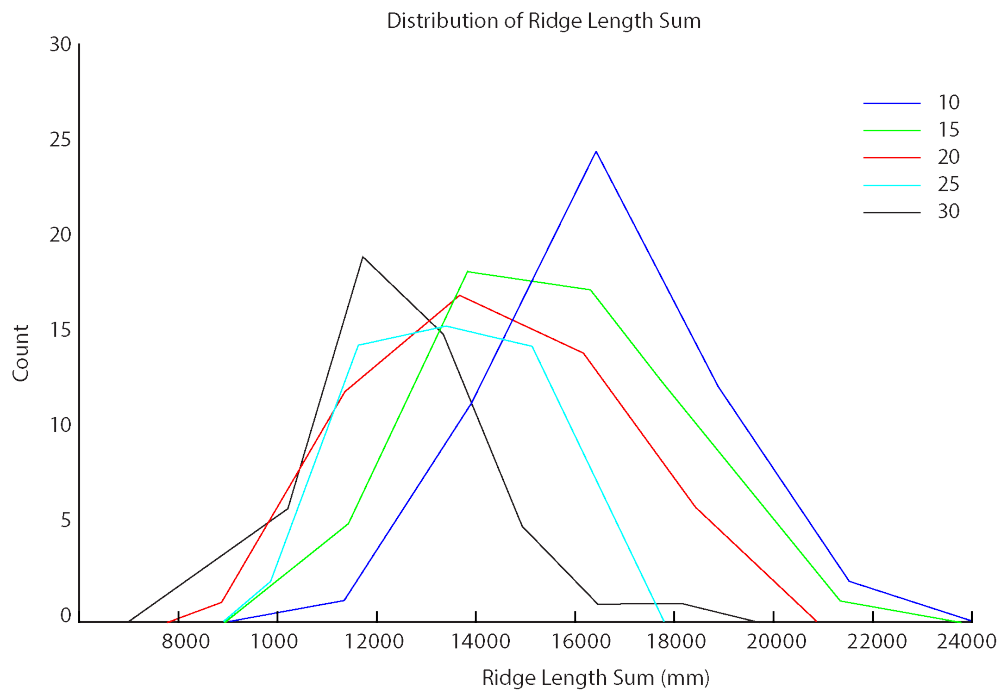


Figure 22- Ridge Length Distribution from Edge Detection Method

By contrast, Figure 22 displays a clear trend that the total ridge length increases with compaction ratio.

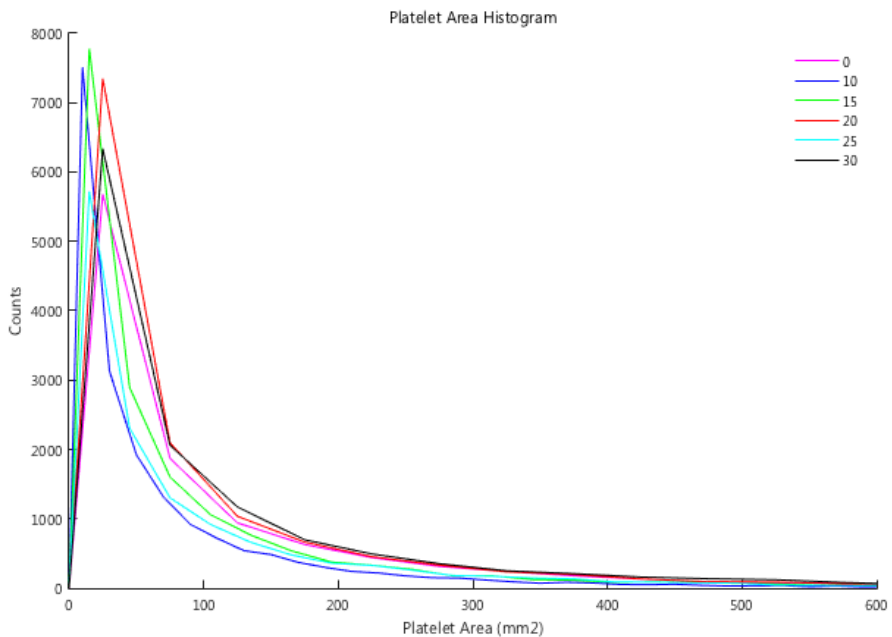


Figure 23- Platelet Area Histogram.

Figure 23 through to Figure 25 show the distribution of geometric properties obtained from the 3D scanning method. These are Platelet Area, Perimeter, and Adjacency, respectively. It is important to notice that in Figure 24 and Figure 25, there is an abrupt jump in frequency of both platelet and perimeter frequency

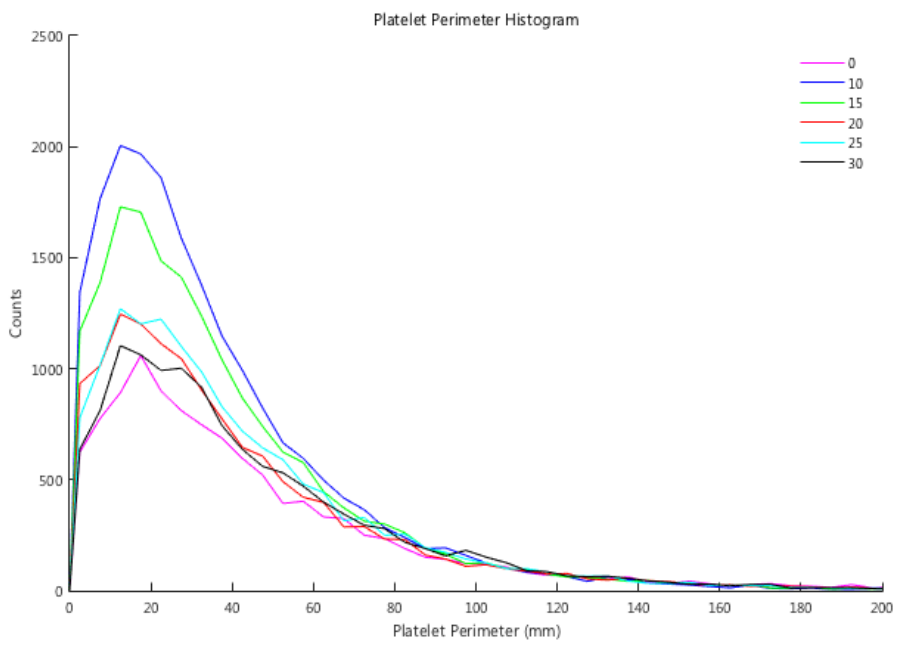


Figure 24- Platelet Perimeter Histogram

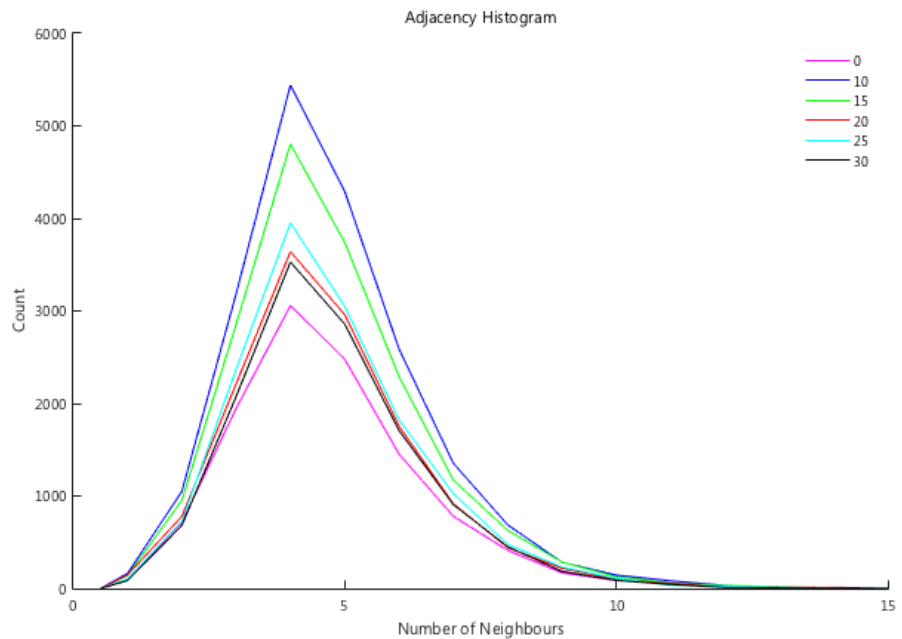


Figure 25- Adjacency Histogram

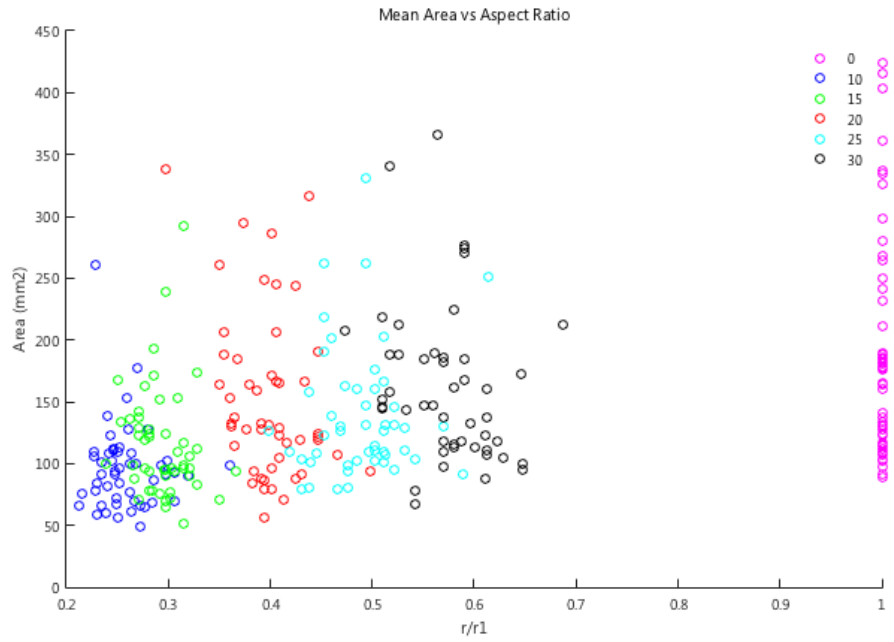


Figure 26- Mean Area vs. Aspect Ratio

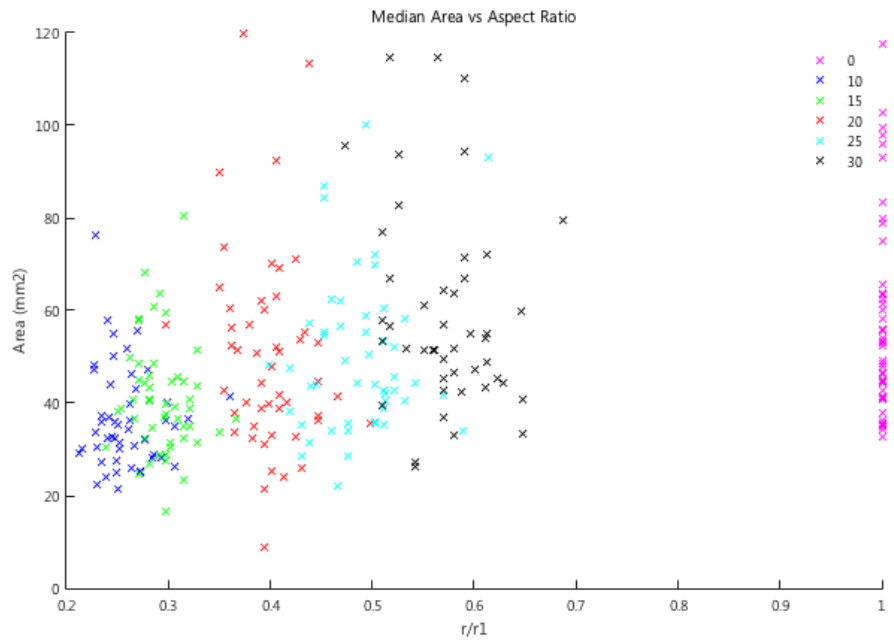


Figure 27- Median Area vs. Aspect Ratio

It can be seen in Figure 26 and Figure 27 that as compaction increases, and hence r/r_1 decreases, the mean and median area decreases, which corresponds to more platelets being formed. Furthermore, it can be seen that the variance increases with r/r_1 . Furthermore, it can be seen that the mean areas are at least three times greater than the medians, which is suggestive of a non-normal distribution.

One-way ANOVA p-values

Group	0	10	15	20	25	30
Perimeter	p<0.001	p<0.001	p<0.001	p<0.001	p<0.001	p<0.001
Area	p<0.001	p<0.001	p<0.001	p<0.001	p<0.001	p<0.001
Diameter	p<0.001	p<0.001	p<0.001	p<0.001	p<0.001	p<0.001
Adjacency	0.9989	0.9974	0.9714	0.8437	0.9886	0.9993
Major Axis	p<0.001	p<0.001	p<0.001	p<0.001	p<0.001	p<0.001
Minor Axis	p<0.001	p<0.001	p<0.001	p<0.001	p<0.001	p<0.001

Table 3- Intragroup ANOVA p-values

ANOVA was conducted on each compaction ratio to test the null hypothesis that the mean value of a geometric property was the same across samples within each compaction ratio. Apart from Adjacency, ANOVA suggests that there is a significant statistical difference in all geometric measures across samples, as evidenced by a p-value far less than 0.05.

8| DISCUSSION

In order to characterise the mechanical behaviour of crumpled paper balls, the trends that exist in the geometry must be related to Force-displacement data. Previous literature has made suggestions and conclusions as to what geometric trends and distributions should be observed, and as such, it seemed prudent to confirm or refute their hypotheses, and explain any discrepancies.

8.1| PRINCIPAL ASSUMPTION

Inherent to the analyses conducted in this thesis and in those of researchers, are a number of inaccuracies and uncertainties introduced by assumptions. The foremost of these assumptions is the definition of a ridge; it is usually defined as a straight line between two nodes. This is empirically difficult to observe, as a straight line observed on a large scale may in fact be a jagged line when observed on a small scale. Whether these situations should be defined as multiple infinitesimally small ridges or one ridge is unclear. However, should there be an infinite number of ridges of effectively zero length, all ridges have effectively identical properties and thus causes the data to become unusable.

Most researchers tend to take the most basic approximation to the ridge network that can be drawn, as seen below in Figure 28. Much like the 3D scanning method developed herein, Andresen created an elevation map of his samples, for which he found the ridge network.

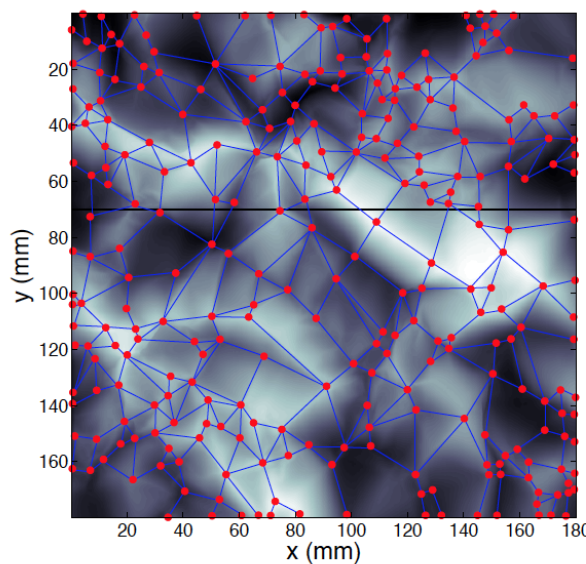


Figure 28- Andresen's Ridge Network Trace

As such, it is important to note that most of the measurements taken of geometry are approximations to the actual behaviour, but the extent of the approximation is uncertain.

In the case of the 3D scanning method, it can be seen that neighbours may share a boundary that consists of more than one line segment, as not all facets are convex polygons. Such a situation is where the definition of a ridge becomes ambiguous, as ridges are loosely defined as the boundaries between facets. However, as the boundaries may consist of two or more distinct segments, one could argue that the boundary consists of two or more "ridges", meaning that ridges must be straight segments. This definition is problematic, as it is uncertain whether the ridges are truly straight, or upon what scale is it appropriate to consider the ridges as being straight.

The two methods developed throughout this thesis have different assumptions as to what constitutes a ridge. The 3D scanning method does not directly look for such ridges, but its result is conveniently similar to approximating a ridge network. However, the 2D edge detection method does look for ridges, albeit indirectly. Particularly, this method defines the ridges as sudden changes in brightness, due to shadows formed along a ridge.

8.2| DISTRIBUTION OF RIDGE LENGTHS AND AREAS

It was hypothesised by Deboeuf and Blair & Kudrolli that the distribution of ridge lengths follows a purely lognormal relationship, whilst Andresen and Lin suggested that whilst a lognormal fits the small scale parts of the ridge length distribution, a power law better fits the large scale part of the distribution.

As we were unable to directly measure the lengths of individual ridges, it was hypothesised that the distribution of the perimeter of the platelets is approximately proportional to the distribution of individual ridge lengths.

We believed this to be a valid assumption based upon the fact that all perimeters will double count part of other perimeters, and that across all samples, the mean ratio of the Major Axis Length to the Minor Axis Length was 2.55, with a standard deviation of 0.19. Furthermore, the median number of neighbours changed very little (See Figure 25). This implies two results; the first is that all platelets tend to have the same number of sides, although these sides may not be perfectly straight, regular lines. The second is that these platelets tend to be in the same proportions.

This assumption is best illustrated by an example:

Side length x	Diagram	Total Length	Perimeter	Total Ridge Length
Aspect ratio a			Length	
2		4ax		12ax
3			36ax	24ax
n			$4n^2ax$	$2ax(n^2+n)$

Table 4- Explanation of Perimeter to Ridge Length Proportionality

Therefore, $\frac{\text{Total Perimeter}}{\text{Total Ridge Length}} = \frac{2n^2}{n^2+n}$. As n becomes very large, the limit is 2, implying that perimeters and ridge lengths are approximately proportional to each other.

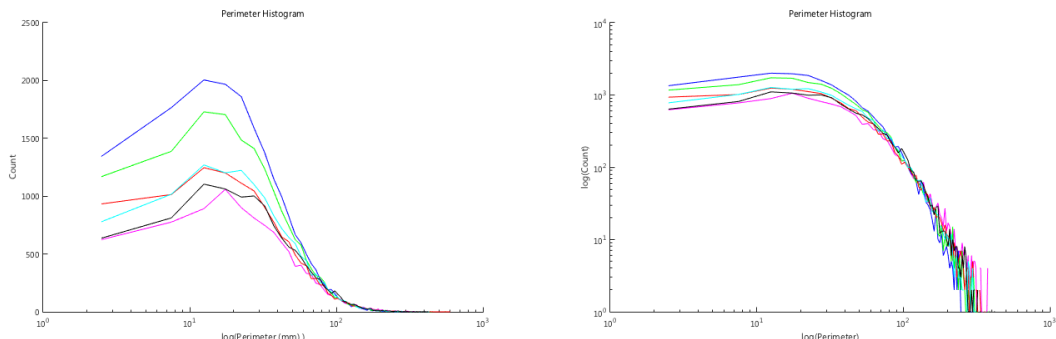


Figure 29- log Perimeter (left)

Figure 30- log-log Perimeter (right)

Despite this assumption, it is inconclusive whether the data fits a lognormal-power relationship, as seen in the above plots. Should a variable have a lognormal distribution, it should appear normally distributed on a log-plot, whilst a power law displays linearity on a log-log plot. The log-log plot suggests some linear trend towards the tail, but increases in variation. When applying a fit against the raw data, it was found that a power law probability distribution fit the data well with $p(l) \propto (1 - \frac{l}{l_{max}})^{0.90}$ for the untested samples, whereas

Andresen's exponent was 0.81. The exponent was found to increase slightly as compaction ratio increased. That is, as the samples become more compacted, their exponent decreases.

We believe that this exponent is a function of material properties, sheet proportions and degree of compaction. A lower exponent suggests a thinner, more plastic material for the same sheet size, or one that has undergone more compaction, as many small lengths have been formed. The apparent discrepancy between Andresen's results and our own results may have been in how vigorously we crumpled the paper. Unfortunately, due to the non-reproducible nature of hand-crumpling, we are unable to directly compare our results with Andresen's. However, we may suggest that the discrepancy between the uncompacted samples could be due to the fact that our samples were allowed to undergo stress-relaxation for 10 days, whereas it does not appear that Andresen allowed for this.

Had our samples been uncrumpled immediately after crumpling, we may have found a greater number of smaller ridges, which would have reduced the exponent.

Due to bin sizing and resolution of the data, it is uncertain if a lognormal distribution is appropriate for the small-scale regions.

As both groups of authors agreed on the lognormal fit of ridge length distribution, the lack of clear evidence in our data may be reflective of the limit of precision in our image processing techniques, especially at very fine resolutions. Refer to pg51 for discussion of limitations.

This may be explained by the fact that when Grasshopper generates the elevation map, it must convert the normalised height value, which is highly precise, into an integer between 0 and 255, thereby losing precision. If this method were to be further explored, generating a matrix of floating point numbers for MATLAB's Watershed function to analyse would be a high priority. Although choosing to convert the normalised height into an image was advantageous for data storage and handling, we believe that it does not lose too significant precision. For unfolded samples that undulated by approximately 50mm due to the permanent deformations, $50\text{mm}/256 \text{ integers} = 0.195\text{mm}$, which is close to the instrument's precision of $\pm 0.1\text{mm}$.

Further utilising the proportionality of perimeter and ridge length assumption, we attempted to apply Balankin's result: $\bar{l} = r_0 \left(\frac{t}{r_0}\right)^\theta \left(\frac{r}{r_0}\right)^\alpha$, which simplifies to the linear relationship:

$\log \bar{l} = (1 - \theta - \alpha) \log r + \theta \log t + \alpha \log r_0$, which reduces to $\log \bar{l} = A \log r + B$, as r_0 , t , θ , and α are all constants. The mean ridge length was taken to be $\bar{l} = \text{mean}(\frac{\text{Perimeter}_i}{\text{Adjacency}_i})$. The results below show that this is a poor fit for our data, as the relationship only explains 15.56% of the

variance in ridge length. These exponents describe the effect that original sheet size and degree of compaction has upon the mean ridge length, and are likely to be material and process dependent.

Regression for Balankin's model of Mean Ridge Length

Variable	Coefficient	p-value of Coefficient
Intercept	1.5015	3.084×10^{-30}
r_{final}	0.2651	1.131×10^{-10}
R^2	0.1546	
α	0.8328	
θ	0.4323	

Table 5- Balankin's model for Mean Ridge Length.

Balankin's result seems somewhat erroneous to begin with, as by assuming that there is a mean value for ridge length implies that ridges are normally distributed. As per Figure 29 and Figure 30, the evidence does not suggest a normal distribution. Balankin's result may be dependent on both the centre of the data as well as its spread, which the mean is partially able to capture, but is nonetheless an incorrectly used statistic.

The distribution of Platelet Areas was found and compared to Andresen's findings. Andresen normalised each sample's areas by the maximum area, and the mean for each sample was found. It is uncertain how Andresen found a fit with $\sigma=1.17$ and $\mu=2.16$ when the logarithm of a normalised value is always negative. Nonetheless, using the same procedure, our data was well fit by a lognormal distribution with parameters $\sigma=0.384$ and $\mu=-2.702$.

When fitting the raw data, however, the lognormal distribution does not seem to fit very well. The parameters for the best fit were $\sigma=2.089$ and $\mu=-4.076$, as seen in Figure 31.

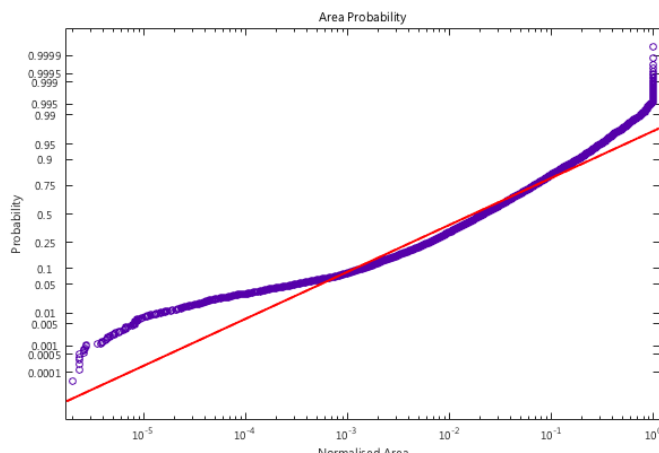


Figure 31- Area Probability Plot for uncompacted samples

No other distribution fitted the raw data well, with all compaction ratios displaying very similar trends. This may suggest that either that the platelet areas do not follow a known distribution, or that the data lost in the image processing had significant impact upon the areas detected. For comparison of all compaction ratios, refer to pg67. The distribution seen shows that the probability of smaller areas is underestimated by a lognormal fit. This may indicate that the hierarchical process of breaking facets into smaller areas no longer applies once a critical value is reached. Potentially, this critical value of area may correspond to the point when material yield rather than buckling of plates becomes the governing mechanism.

8.3| FORCE AND ENERGY PROPORTIONALITY

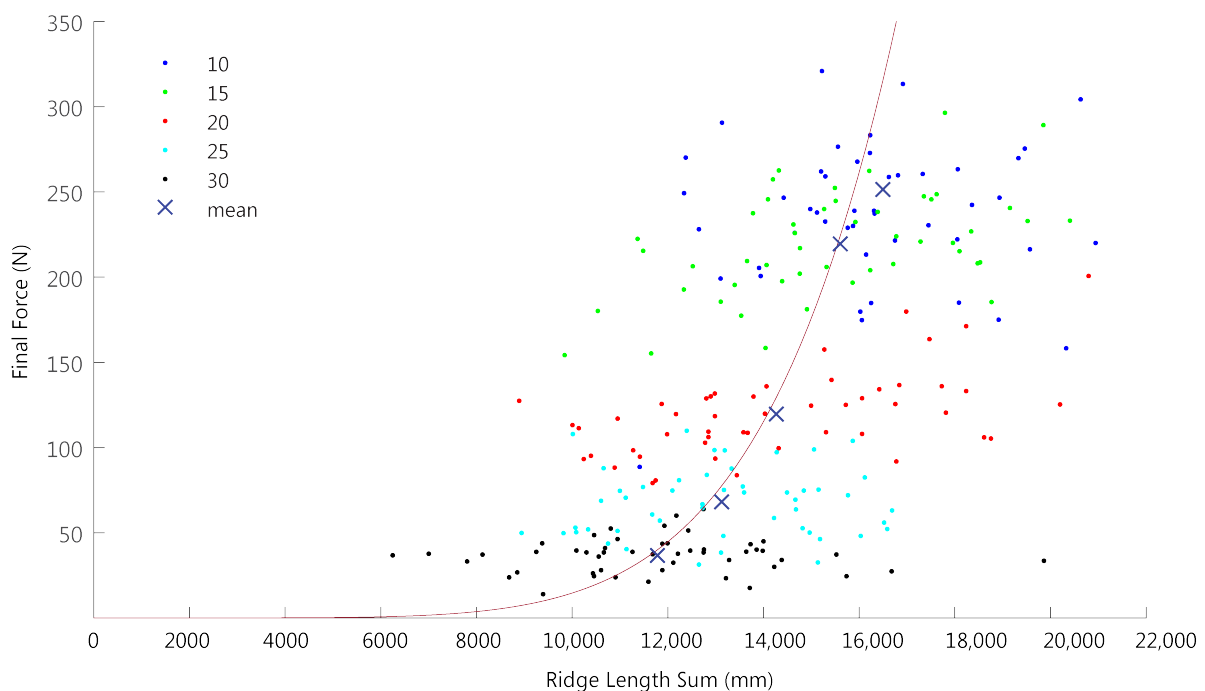


Figure 32- Final Force vs. Total Ridge Length

A first order analysis suggests a poorly fitted exponential relationship between force and ridge length sum, which is suggested in the diagonally upward trend, exhibited in Figure 32. The ridge length sum was taken from the 2D edge detection method, as the 3D scanning method produced a result that was believed to be logically inconsistent. That is, one could reasonably expect the mean ridge length sum to increase with compaction, but what was observed was a drop in mean total ridge length in one of the groups. This seemed to be an unlikely natural phenomenon, and was hence disregarded in favour of the above data. We propose that the exponent is a function of stiffness and strength on material, local, and global scales.

Researchers have typically treated ridges like beams; long and slender beams will have a tendency to bend or buckle, whereas short beams will yield before buckling.

The crumpling process tends to reduce the length of ridges, either by intersection with other ridges, or buckling of present ridges. This means that the behaviour becomes more materially dependent as the compaction process continues.

The crumpled balls fluctuate between dynamic and static states as each ridge buckles into a more stable configuration, which implies that the geometry itself is a function of the geometry. This means that the relationship is in fact an iterative second order effect, for which a first order linear analysis such as this is inappropriate.

Nonetheless, it is reasonable to hypothesise that the exponent is an increasing function of stiffness and strength for the following reasons:

- A higher material strength means that ridges may absorb more energy, requiring fewer ridges to resist a given force.
- A higher material stiffness implies that the local ridge strength increases, hence an increase in global strength, provided that buckling is the governing behaviour.
- A higher local stiffness implies a higher local strength, as both are functions of constant material stiffness/strength and variable local geometry.
- The exponent must be an increasing function of both properties as a negative exponent implies that the maximum force is reached with no ridges; an uncrumpled sheet of paper, which is clearly not the case.

Fundamentally, by attempting to relate Total Ridge Length to Energy or Force, there is an assumption that the energy or force is shared equally throughout the network of ridges.

This is not necessarily the case, as shorter ridges have a higher energy density due to their higher buckling capacity and the cumulative work that formed the ridge. Furthermore, when the ridges and platelets buckle, they are not able to resist any load until they reach a stable configuration. This means that the load they were previously carrying must redistribute itself to a different series of pathways through the ridge network. This implies that the stress distribution is constantly changing, and therefore it cannot be assumed that all of the ball's geometry is actually contributing to resisting the load. Therefore, analysing all of the geometry under the assumption that all of it contributes may not fully capture the behaviour.

8.4| ENERGY AS A FUNCTION OF GEOMETRY

Though Table 3 showed that the means were significantly different across samples within a compaction ratio, it was expected that each group would be statistically distinct. Otherwise, it can be concluded that compaction has no effect upon geometry or mechanical behaviour.

Table 6 shows that each compaction ratio is a statistically distinct group, as the p-values are less than 0.05.

One-way ANOVA p-values

Total Ridge Length	p<0.001
Total Energy	p<0.001
Maximum Force	p<0.001
Maximum Displacement	p<0.001
Final r/r ₀	p<0.001
Final r/r ₁	p<0.001

Table 6-Intergroup ANOVA p-values

As such, it was deemed appropriate to perform a regression dependent upon the compaction ratio groupings, the results of which are seen below in Table 7 and Table 8.

The purpose of this regression was to establish the smallest group of geometric parameters that may be able to explain the force-displacement data that was collected. If strong relationships exist, an accurate prediction of the mechanical performance becomes possible, which is a critical step towards designing a crumpled structure.

Generalised Linear Model- Total Energy

Variable	Coefficient	p-value of Coefficient	Adjusted Coefficient
Intercept	5.355	p<0.001	5.355
r/r ₀	1.862	p<0.001	1.862
r/r ₁	-4.530	p<0.001	-4.530
Mean Area	0.002	0.030	0.002
Median Area	0.004	0.293	0
Mean Adjacency	-0.587	0.039	-0.587
Median Adjacency	0.018	0.682	0
Mean Perimeter	-0.007	0.356	0
Median Perimeter	-0.019	0.129	0
Total Ridge Length	7.07E-05	0.006	7.07E-05
R ²	0.8354		-0.0744

Table 7- Generalised Linear Model- Total Energy

Generalised Linear Model- Maximum Force

Variable	Coefficient	p-value of Coefficient	Adjusted Coefficient
Intercept	674.983	0.003	674.983
Final r/r ₀	236.561	p<0.001	236.561
Final r/r ₁	-591.958	p<0.001	-591.958
Mean Area	0.224	0.045	0.224
Median Area	0.329	0.576	0
Mean Adjacency	-69.566	0.127	0
Median Adjacency	4.967	0.479	0
Mean Perimeter	-1.260	0.278	0
Median Perimeter	-1.834	0.359	0
Total Ridge Length	0.008	0.062	0
R ²	0.7746		-11.7458

Table 8- Generalised Linear Model- Maximum Force

As many of the p-values for the regression coefficients were greater than 0.05, it demonstrates that certain variables appear to have no effect upon the force or energy and thus don't belong in the model. Thus, the coefficients that have $p>0.05$ must be made zero. Obviously, this changes the results of the regression quite significantly, as seen in the very large R^2 values in Table 7 and Table 8. Nevertheless, the results indicated which independent variables should be included in the regression model.

As Mean Area appears in both regressions, it is likely that most other geometric properties have some form of relationship to area. It is theorised that perimeters and ridges must continually break down to form smaller platelets until a limiting size is reached, when the platelets no longer buckle. At this critical size, it becomes inefficient to form any further subdivisions, and hence the platelet area becomes the limiting factor.

When another regression was performed, it was found that Mean Area also dropped out of the regression.

The subsequent regressions performed linearly related the logarithm of energy and force to compaction ratio and aspect ratio. This results in an exponential relationship, as

$\log y = Ax + By + C$ is equivalent to $y = De^{Ax+By}$. This was chosen as the shape of the force-displacement curves display increasingly concave up curvature, which is indicative of power-law relationships of degree greater than two or exponential relationships.

Reduced Generalised Linear Model- Logarithm of Total Energy

Variable	Coefficient	p-value of Coefficient	Adjusted Coefficient
Intercept	2.671	$p<0.001$	2.671
r/r_0	-2.795	$p<0.001$	-2.795
r/r_1	-6.776	$p<0.001$	-6.776
R^2	0.9795		0.9795

Table 9- Reduced Generalised Linear Model- logarithm of Total Energy

$$\text{This yields: } E = 14.453e^{-2.796\frac{r}{r_0} - 6.776\frac{r}{r_1}}$$

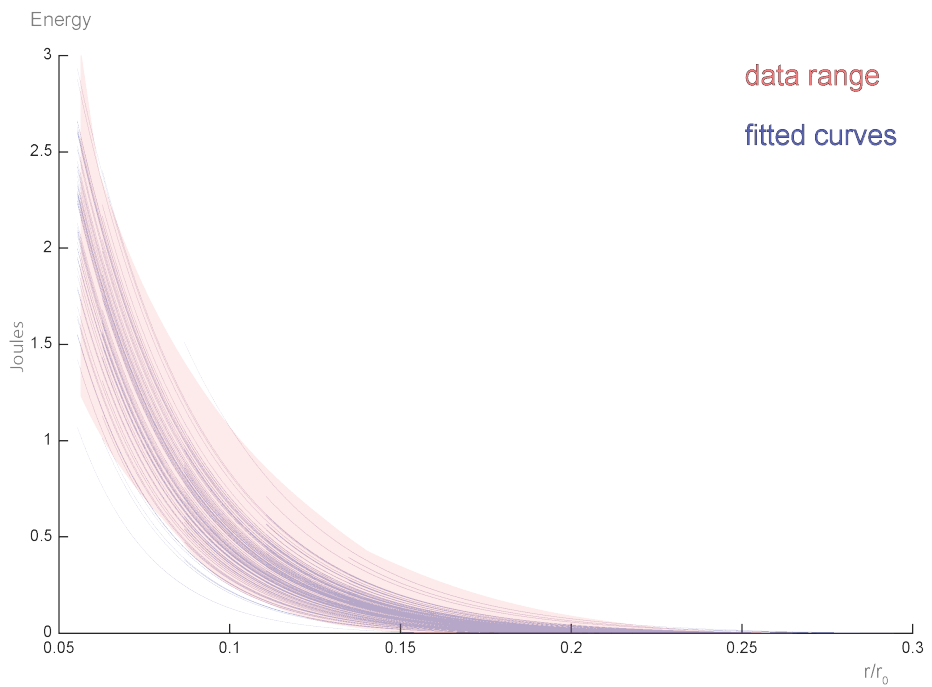


Figure 33- Energy Relationship

Reduced Generalised Linear Model- Logarithm of Maximum Force

Variable	Coefficient	p-value of Coefficient	Adjusted Coefficient
Intercept	7.980	p<0.001	7.980
r/r₀	-8.350	p<0.001	-8.350
r/r₁	-6.509	p<0.001	-6.509
R²	0.9748		0.9748

Table 10- Reduced Generalised Linear Model- Logarithm of Maximum Force

$$\text{This yields: } F = 2923e^{-8.350\frac{r}{r_0} - 6.509\frac{r}{r_1}}$$

It can be seen that aspect ratio's coefficient was approximately 250% of compaction ratio's coefficient for energy, but only about 80% of compaction ratio's coefficient for force. This is believed to mean that the crumpling process prior to load testing has significant impact upon the formation of microscale geometries, and hence the mechanical behaviour.

The difference in magnitude of these coefficients may be attributed to the fact that a unit change in compaction ratio is a far larger displacement than a unit change in aspect ratio. This is likely due to the fact that force is a function of displacement, whereas energy is a function of displacement squared.

Thus, changes in compaction ratio have a greater effect upon maximum force, whereas changes in aspect ratio have a larger effect upon energy. It is theorised that this is because aspect ratio describes the strain of the specimen, whilst compaction ratio may be a good measure of how much friction and fold interlock can occur.

8.5| LIMITATIONS AND ERRORS

Throughout the experimentation and analysis process care was taken to prevent the introduction of systemic errors and related inaccuracies.

The techniques described herein, have a number of limitations that due to time, software, and capability constraints, were unable to be fully rectified. Nonetheless, the techniques are believed to be quite reliable, reproducible, and a reasonable approximation to reality.

8.5.1| SPECIMEN PREPARATION

As the specimens were hand crumpled by two different people, crumpling method may have become a variable. However, as a large number of samples were tested, any randomness introduced by two potentially different methods is likely to have been smoothed out. Some research suggests that crumpling method does not affect the outcomes, whilst other research states that it does. A concurrent thesis project suggests that crumpling method does affect certain outcomes, whilst the effect that different crumpling methods have upon other outcomes remains indistinguishable.

8.5.2| TESTING

During testing, human error can be significant, as evidenced by the need to confirm whether our samples had been switched, which they had. This may have been due to a storage error with the samples.

Testing the samples axially is quite a time consuming process and may not necessarily be the most efficient means by which to gain mechanical data. Potentially, a far faster load rate may be more applicable to simulate the desired impact loads for which there is strong potential in the use of crumpled structures. However, the accuracy of such tests is quite high, as the MTS Criterion 40 is able to measure to a precision of $\pm 0.00005\text{mm}$.

8.5.3| 3D SCANNING

The Artec3D Spider scanner is a very accurate instrument, with a precision of $\pm 0.1\text{mm}$. The error in the 3D scanning process arises when the samples are uncrumpled. Potentially, some ridges may be flattened out, or new ridges introduced. Furthermore, as a sensitivity analysis was not conducted, the effect that the 3D Processing Algorithms had upon the result of the geometric analyses is uncertain. Once again, this process is highly time-consuming.

8.5.4| ELEVATION MAPPING

Elevation mapping potentially reduces the accuracy of the data in a significant manner, as each normalised height value must be converted into an integer between 0 and 255 in order to be mapped into an image. If a specimen is quite flat when scanned, the detail will be preserved more effectively than if the specimen undulated significantly.

8.5.5| MATLAB

Whilst MATLAB's analysis of the elevation image was reliable and accurate for the data that it received, the actual generation of the ridge image was not as reliable. MATLAB's Watershed function was able to approximate the ridge network to a certain extent, but some ridges remained undetected. This is due to different definitions of ridges that for the most part coincide. We were looking for all folds in the sheet, whereas MATLAB determines regions that drain to the same point. Unfortunately, due to the way the Watershed function works, there was no threshold that could be changed that would force MATLAB to detect those ridges. Potentially, if all the ridges were detected, the geometric distributions could become more right skewed as a larger number of small ridges would be detected, but would likely to remain of the same type of distribution. It is therefore unlikely to change the conclusions reached. Furthermore, as there were a significant number of elevation maps that were batch processed, it was impractical to check each individual ridge image against the physical sample.

8.5.6| 2D SCANNING

The flatbed scans of the uncrumpled sheets can be quite precise, with a precision of 250DPI (approximately 10 pixels per millimetre). However, the Neon Edge detection function may not detect all the ridges, or may include areas that are not ridges. This function requires input parameters, which were determined visually to be the most suitable, but whether they were the most suitable for the subsequent image processing is not known.

8.5.7| GRASSHOPPER IMAGE SAMPLING

In the form that the grasshopper script was when used to obtain data, error may have arisen from the fact that the circles were populated in a grid and resized based upon the pixel brightness. Whilst this was uniform over all samples tested and was calibrated by knowing the exact length of one entire network, errors may have been reduced if clusters of circles that were not constrained to a grid populated the areas.

9| CONCLUSIONS

In conclusion, it has been found that the work done by a crumpled paper ball is well described by an exponential relationship dependent upon compaction and aspect ratios.

Whilst loose trends in the uncrumpled geometric data exist, the spread is significant such that it cannot be an accurate predictor of the mechanical performance of a crumpled paper ball.

Two different geometric analysis techniques were developed, which displayed results consistent with previous research. These techniques were effective in gaining understanding of the trends present in uncrumpled sheets, but require modification to accurately describe the real geometries.

Furthermore, it can be concluded that an analysis of an uncrumpled sheet is insufficient to attempt to correlate geometry with mechanical performance. The trends in the data suggest that the individual geometric features play a significant role in the macroscale behaviours, but the interaction in full three-dimensionality is equally, if not more significant. Thus, it is recommended that three-dimensional analyses be the focus of further investigation.

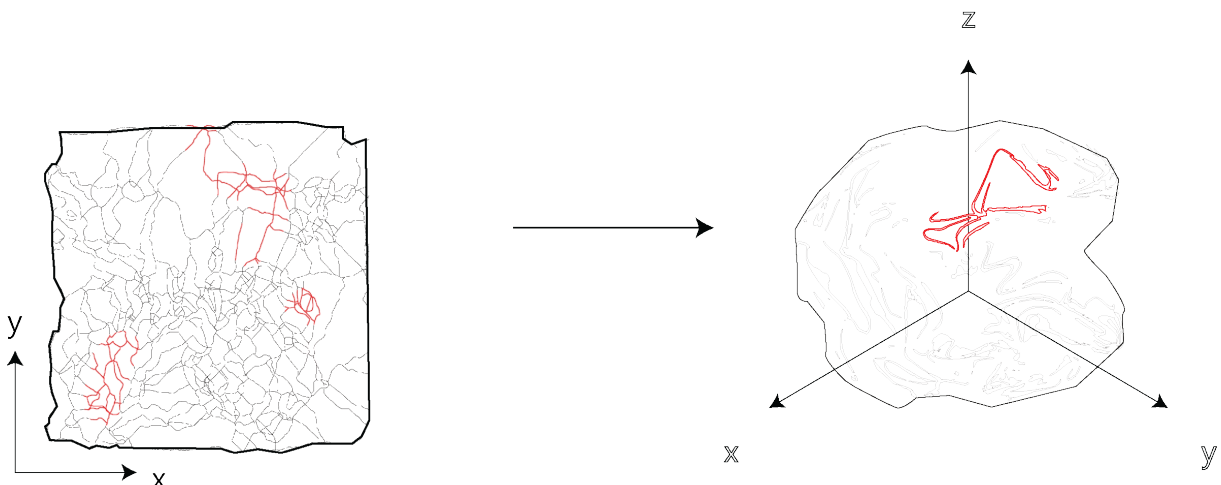


Figure 34- 3D analysis

These three-dimensional analyses should focus on the interactions between microscale geometries, particularly the roles that friction and interlock have in determining mechanical properties. In addition to this, it is recommended that the analysis not be conducted on a frame-by-frame basis, but rather as one continuous process, with many second order effects.

10| REFERENCES

- Aharoni, H. & Sharon, E., 2010. Direct observation of the temporal and spatial dynamics during crumpling. *Nature materials*, 9(12), pp.993–997. Available at: <http://dx.doi.org/10.1038/nmat2893>.
- Ben Amar, M. & Pomeau, Y., 1997. Crumpled paper. *Proceedings of the Royal Society A: Mathematical, Physical and Engineering Sciences*, 453(1959), pp.729–755.
- Andresen, C.A., Hansen, A. & Schmittbuhl, J., 2007. Ridge network in crumpled paper. *Physical Review E - Statistical, Nonlinear, and Soft Matter Physics*, 76(2).
- Bai, W. et al., 2010. Scaling relation for a compact crumpled thin sheet. *Physical Review E - Statistical, Nonlinear, and Soft Matter Physics*, 82(6), pp.1–5.
- Baillie, C.F. & Johnston, D. a., 1991. Crumpling dynamically triangulated random surfaces in two dimensions. *Physics Letters B*, 258(3-4), pp.346–352.
- Baillie, C.F. & Johnston, D. a., 1992. Effective model for crumpling in two dimensions? *Physical Review D*, 46(10), pp.4761–4764.
- Balakin, A.S. et al., 2013. Fractal features of a crumpling network in randomly folded thin matter and mechanics of sheet crushing. *Physical Review E - Statistical, Nonlinear, and Soft Matter Physics*, 87(5), pp.1–11.
- Balakin, A.S., Huerta, O.S. & Tapia, V., 2013. Statistics of energy dissipation and stress relaxation in a crumpling network of randomly folded aluminum foils. , 032402, pp.1–7.
- Balakin, A.S., De Oca, R.C.M. & Ochoa, D.S., 2007. Intrinsically anomalous self-similarity of randomly folded matter. *Physical Review E - Statistical, Nonlinear, and Soft Matter Physics*, 76(3), pp.76–79.
- Bevilacqua, L., 2004. Fractal balls. *Applied Mathematical Modelling*, 28(6), pp.547–558.
- Blair, D.L. & Kudrolli, A., 2005. Geometry of crumpled paper. *Physical Review Letters*, 94(16).
- Bouaziz, O. et al., 2013. Compression of crumpled aluminum thin foils and comparison with other cellular materials. *Materials Science and Engineering A*, 570, pp.1–7.
- Cambou, A.D. & Menon, N., 2011. Three-dimensional structure of a sheet crumpled into a ball. *Proceedings of the National Academy of Sciences of the United States of America*, 108(36), pp.14741–14745.
- Deboeuf, S. et al., 2013. Comparative study of crumpling and folding of thin sheets. *Physical Review Letters*, 110(10), pp.1–5.
- Didonna, B., 2006. Crumpling: A look inside the creases. *Nature Materials*, 5(3), pp.167–168.

- DiDonna, B. a., 2002. Scaling of the buckling transition of ridges in thin sheets. *Physical Review E - Statistical, Nonlinear, and Soft Matter Physics*, 66(1).
- Efrati, E. et al., 2014. Confined disclinations: exterior vs material constraints in developable thin elastic sheets. , 1, pp.1–8.
- Lin, Y.C. et al., 2009. X-ray tomography of a crumpled plastoelastic thin sheet. *Physical Review E - Statistical, Nonlinear, and Soft Matter Physics*, 80(6), pp.1–6.
- Lobkovsky, A.E. & Witten, T. a., 1996. Properties of Ridges in Elastic Membranes. , p.13. Available at: <http://arxiv.org/abs/cond-mat/9609068>.
- Peraza-Hernandez, E. a et al., 2014. Origami-inspired active structures: a synthesis and review. *Smart Materials and Structures*, 23(9), p.094001. Available at: <http://stacks.iop.org/0964-1726/23/i=9/a=094001?key=crossref.6226c53c3ab2492e5686c0d4be08ea2e>.
- Quach, S., 2014. The Characterisation of Compressed Crumpled Structures. , (October 2014), pp.1–79.
- Tallinen, T., Aström, J. a & Timonen, J., 2009. The effect of plasticity in crumpling of thin sheets. *Nature materials*, 8(1), pp.25–29. Available at: <http://dx.doi.org/10.1038/nmat2343>.

11| APPENDICES

11.1| MATLAB IMAGE PROCESSING CODE

11.1.1| WATERSHED CODE

```
%% PREPARATION
Pixel_length=input('What width does 1 pixel in the photo represent in reality?');
tic;
Pixel_area=Pixel_length^2;

% list all data files in current directory
f = dir('*.*');

%% PREALLOCATION
%functional vectors
M=cell(length(f),1);
M_water=cell(length(f),1);
masked_M_comp=cell(length(f),1);
STATS=cell(length(f),1);
adj=cell(length(f),1);

% Data Vectors
Area=cell(length(f),1);
Perimeter=cell(length(f),1);
Extent=cell(length(f),1);
EquivDiameter=cell(length(f),1);
MajorAxisLength=cell(length(f),1);
MinorAxisLength=cell(length(f),1);
total_ridge_length=zeros(length(f),1);
Adjacency=cell(length(f),1);

%% ANALYSIS
for i=1:length(f),
    % echo i;
    tempread=imread(f(i).name);

    %convert to greyscale image
    M{i}=rgb2gray(tempread);

    %Mountain watershed segmentation
    M_water_mountain=watershed(M{i});
    M_water_mountain=M_water_mountain ==0;

    %valley watershed segmentation
    %invert image
    M_comp=imcomplement(M{i});

    %binary image mask
    bw=im2bw(M_comp,0.9999);
    bw2=bwareaopen(bw,15000);
    bw3=imcomplement(bw2);
    masked_M_comp{i}=bsxfun(@times,M_comp,cast(bw3,'uint8'));

    M_water_valley=watershed(masked_M_comp{i});
    M_water_valley=M_water_valley ==0;
```

```

%prepare filepaths
filename11=cat(2,'mountain_watershed',num2str(i));
filename1=cat(2,filename11,'.png');
filepath1=cat(2,'/Users/Beton/Documents/MATLAB/3d
data/watershed/mountain/',filename1);
imwrite(M_water_mountain,filepath1,'png');

filename22=cat(2,'valley_watershed',num2str(i));
filename2=cat(2,filename22,'.png');
filepath2=cat(2,'/Users/Beton/Documents/MATLAB/3d
data/watershed/valley/',filename2);
imwrite(M_water_valley,filepath2,'png');

filename33=cat(2,'watershed',num2str(i));
filename3=cat(2,filename33,'.png');
filepath3=cat(2,'/Users/Beton/Documents/MATLAB/3d
data/watershed/',filename3);

%combine images
img_comp=imadd(M_water_valley,M_water_mountain);
img_write=imcomplement(img_comp);
img=cast(imcomplement(img_comp),'uint8');
M_water{i}=cast(labelmatrix(bwconncomp(img)), 'double');

%write combined image
imwrite(img_write,filepath3,'png');

STATS{i}=regionprops(M_water{i}, 'Area', 'Extent', 'EquivDiameter', 'MajorAxisL
ength', 'MinorAxisLength', 'Perimeter');

%preallocate
Area{i,1}=zeros(length(STATS{i}),1);
Perimeter{i,1}=zeros(length(STATS{i}),1);
Extent{i,1}=zeros(length(STATS{i}),1);
EquivDiameter{i,1}=zeros(length(STATS{i}),1);
MajorAxisLength{i,1}=zeros(length(STATS{i}),1);
MinorAxisLength{i,1}=zeros(length(STATS{i}),1);

%extract data
for j=1:length(STATS{i})
    Area{i,1}(j,1)=STATS{i,1}(j,1).Area*Pixel_area;
    Perimeter{i,1}(j,1)=STATS{i,1}(j,1).Perimeter*Pixel_length;
    Extent{i,1}(j,1)=STATS{i,1}(j,1).Extent;
    EquivDiameter{i,1}(j,1)=STATS{i,1}(j,1).EquivDiameter*Pixel_length;
    MajorAxisLength{i,1}(j,1)=STATS{i,1}(j,1).MajorAxisLength*Pixel_length;
    MinorAxisLength{i,1}(j,1)=STATS{i,1}(j,1).MinorAxisLength*Pixel_length;
end

%ridge length is the total number of pixels minus the non-black pixels
total_ridge_length(i)=(numel(img)-nnz(img))*Pixel_length;

%adjacency
adj{i}=imRAG(M_water{i});
concatenated=cat(1,adj{i,1}(:,1),adj{i,1}(:,2));
x=unique(concatenated);
N=numel(x);
Adjacency{i}=zeros(N,1);
for k=1:N
    Adjacency{i,1}(k)=sum(concatenated==x(k));
end
end
save('/Users/Beton/Documents/MATLAB/3d_data/variables', '-v7.3');
disp('FINISHED!')
toc

```

11.1.2| IMRAG FUNCTION

Disclaimer: This MATLAB function is not my own work, but it was used in the above function, and should hence be included for future reference.

```
function varargout = imRAG(img, varargin)
%IMRAG Region adjacency graph of a labeled image
%
% Usage:
% ADJ = imRAG(IMG);
% computes region adjacencies graph of labeled 2D or 3D image IMG.
% The result is a N*2 array, containing 2 indices for each couple of
% neighbor regions. Two regions are considered as neighbor if they are
% separated by a black (i. e. with color 0) pixel in the horizontal or
% vertical direction.
% ADJ has the format [LBL1 LBL2], LBL1 and LBL2 being vertical arrays the
% same size.
%
% LBL1 is given in ascending order, LBL2 is given in ascending order for
% each LBL1. Ex:
% [1 2]
% [1 3]
% [1 4]
% [2 3]
% [2 5]
% [3 4]
%
% [NODES, ADJ] = imRAG(IMG);
% Return two arrays: the first one is a [N*2] array containing centroids
% of the N labeled region, and ADJ is the adjacency previously described.
% For 3D images, the nodes array is [N*3].
%
% Example (requires image processing toolbox)
% read and display an image with several objects
% img = imread('coins.png');
% figure(1); clf;
% imshow(img); hold on;
% % compute the Skeleton by influence zones using watershed
% bin = imfill(img>100, 'holes');
% dist = bwdist(bin);
% wat = watershed(dist, 4);
% % compute overlay image for display
% tmp = uint8(double(img).* (wat>0));
% ovr = uint8(cat(3, max(img, uint8(255*(wat==0))), tmp, tmp));
% imshow(ovr);
% % show the resulting graph
% [n e] = imRAG(wat);
% for i = 1:size(e, 1)
%     plot(n(e(i,:)), 1), n(e(i,:)), 2), 'linewidth', 4, 'color', 'g');
% end
% plot(n(:,1), n(:,2), 'bo', 'markerfacecolor', 'b');
%
%
% Create a basic 3D image with labels, and compute RAG
% germs = [50 50 50; ...
%           20 20 20;80 20 20;20 80 20;80 80 20; ...
%           20 20 80;80 20 80;20 80 80;80 80 80];
% img = zeros([100 100 100]);
% for i = 1:size(germs, 1)
%     img(germs(i,1), germs(i,2), germs(i,3)) = 1;
% end
% wat = watershed(bwdist(img), 6);
% [n e] = imRAG(wat);
% figure; drawGraph(n, e);
```

```

%      view(3);
%
%
%
% -----
% Author: David Legland
% e-mail: david.legland@grignon.inra.fr
% Created: 2004-02-20,
% Copyright 2007 INRA - BIA PV Nantes - MIAJ Jouy-en-Josas.

% History
% 2007-10-12 update doc
% 2007-10-17 add example
% 2010-03-08 replace calls to regionprops by local centroid computation
% 2010-07-29 update doc
% 2012-07-20 remove the use of "diff", using less memory

%% Initialisations

% size of image
dim = size(img);

% number of dimensions
nd = length(dim);

% initialize array of neighbor regions
edges = [];

% Number of background pixels or voxels between two regions
% gap = 0 -> regions are contiguous
% gap = 1 -> there is a 1-pixel large line or surface between two adjacent
%   pixels, for example the result of a watershed
gap = 1;
if ~isempty(varargin) && isnumeric(varargin{1})
    gap = varargin{1};
end
shift = gap + 1;

if nd == 2

    %% First direction of 2D image

    % identify transitions
    [i1 i2] = find(img(1:end-shift,: ) ~= img((shift+1):end, :));

    % get values of consecutive changes
    val1 = img(sub2ind(dim, i1, i2));
    val2 = img(sub2ind(dim, i1+shift, i2));

    % keep only changes not involving background
    inds = val1 ~= 0 & val2 ~= 0 & val1 ~= val2;
    edges = unique([val1(inds) val2(inds)], 'rows');

    %% Second direction of 2D image

    % identify transitions
    [i1 i2] = find(img(:, 1:end-shift) ~= img(:, (shift+1):end));

    % get values of consecutive changes
    val1 = img(sub2ind(dim, i1, i2));
    val2 = img(sub2ind(dim, i1, i2+shift));

```

```

% keep only changes not involving background
inds = val1 ~= 0 & val2 ~= 0 & val1 ~= val2;
edges = [edges; unique([val1(inds) val2(inds)]), 'rows')];

elseif nd == 3
%% First direction of 3D image

% identify transitions
[i1 i2 i3] = ind2sub(dim-[shift 0 0], ...
    find(img(1:end-shift,:,:)) ~= img((shift+1):end,:,:,:));

% get values of consecutive changes
val1 = img(sub2ind(dim, i1, i2, i3));
val2 = img(sub2ind(dim, i1+shift, i2, i3));

% keep only changes not involving background
inds = val1 ~= 0 & val2 ~= 0 & val1 ~= val2;
edges = unique([val1(inds) val2(inds)]), 'rows');

%% Second direction of 3D image

% identify transitions
[i1 i2 i3] = ind2sub(dim-[0 shift 0], ...
    find(img(:,1:end-shift,:) ~= img(:,(shift+1):end,:)));

% get values of consecutive changes
val1 = img(sub2ind(dim, i1, i2, i3));
val2 = img(sub2ind(dim, i1, i2+shift, i3));

% keep only changes not involving background
inds = val1 ~= 0 & val2 ~= 0 & val1 ~= val2;
edges = [edges; unique([val1(inds) val2(inds)]), 'rows')];

%% Third direction of 3D image

% identify transitions
[i1 i2 i3] = ind2sub(dim-[0 0 shift], ...
    find(img(:,:,1:end-shift) ~= img(:,:,1:(shift+1):end))));

% get values of consecutive changes
val1 = img(sub2ind(dim, i1, i2, i3));
val2 = img(sub2ind(dim, i1, i2, i3+shift));

% keep only changes not involving background
inds = val1 ~= 0 & val2 ~= 0 & val1 ~= val2;
edges = [edges; unique([val1(inds) val2(inds)]), 'rows')];

end

% format output to have increasing order of n1, n1<n2, and
% increasing order of n2 for n1=constant.
edges = sortrows(sort(edges, 2));

% remove eventual double edges
edges = unique(edges, 'rows');

```

```

%% Output processing

if nargout == 1
    varargout{1} = edges;

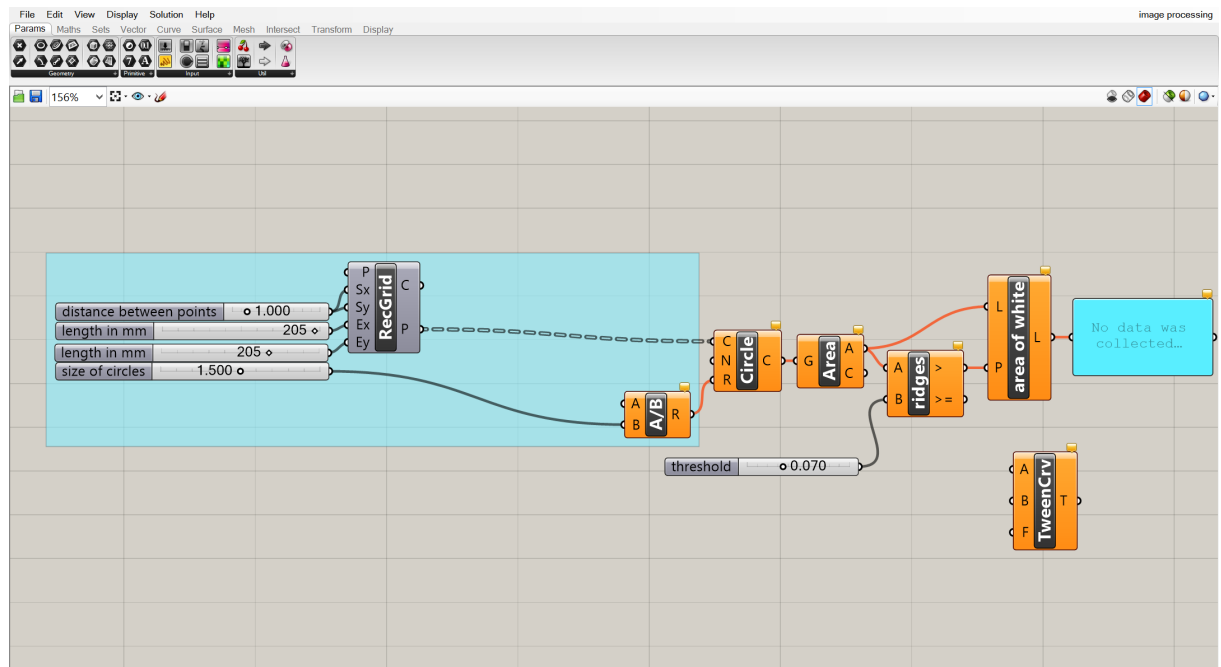
elseif nargout == 2
    % Also compute region centroids
    N = max(img(:));
    points = zeros(N, nd);
    labels = unique(img);
    labels(labels==0) = [];

    if nd == 2
        % compute 2D centroids
        for i = 1:length(labels)
            label = labels(i);
            [iy ix] = ind2sub(dim, find(img==label));
            points(label, 1) = mean(ix);
            points(label, 2) = mean(iy);
        end
    else
        % compute 3D centroids
        for i = 1:length(labels)
            label = labels(i);
            [iy ix iz] = ind2sub(dim, find(img==label));
            points(label, 1) = mean(ix);
            points(label, 2) = mean(iy);
            points(label, 3) = mean(iz);
        end
    end
end

% setup output arguments
varargout{1} = points;
varargout{2} = edges;
end

```

11.2 | 2D EDGE DETECTION GRASSHOPPER DEFINITION



11.3| MANN-WHITNEY U-TESTS

It was planned for the samples to be tested in groups of fifty, however, on the test day, a change of mind was made part way through a group. This was rather lucky, as it enabled the determination of the order the samples were tested in, based upon which groups samples 148-150, 151-153, and 201-203 fall into. Samples were stored in a 10x10 grid.

The Expected Arrangement

Samples 101-200

30	30	30	30	30	30	30	30	30	30
30	30	30	30	30	30	30	30	30	30
30	30	30	30	30	30	30	30	30	30
30	30	30	30	30	30	30	30	30	30
30	30	30	30	30	30	30	30	30	30
15	15	15	25	25	25	25	25	25	25
25	25	25	25	25	25	25	25	25	25
25	25	25	25	25	25	25	25	25	25
25	25	25	25	25	25	25	25	25	25
25	25	25	25	25	25	25	25	25	25

Samples 201-250

25	25	25	15	15	15	15	15	15	15
15	15	15	15	15	15	15	15	15	15
15	15	15	15	15	15	15	15	15	15
15	15	15	15	15	15	15	15	15	15
15	15	15	15	15	15	15	15	15	15
0	0	0	0	0	0	0	0	0	0
0	0	0	0	0	0	0	0	0	0
0	0	0	0	0	0	0	0	0	0
0	0	0	0	0	0	0	0	0	0
0	0	0	0	0	0	0	0	0	0

The Alternate Arrangement- Rotated 180 degrees

Samples 101-200

25	25	25	25	25	25	25	25	25	25
25	25	25	25	25	25	25	25	25	25
25	25	25	25	25	25	25	25	25	25
25	25	25	25	25	25	25	25	25	25
25	25	25	25	25	25	25	25	15	15
30	30	30	30	30	30	30	30	30	30
30	30	30	30	30	30	30	30	30	30
30	30	30	30	30	30	30	30	30	30
30	30	30	30	30	30	30	30	30	30
30	30	30	30	30	30	30	30	30	30

Samples 201-250

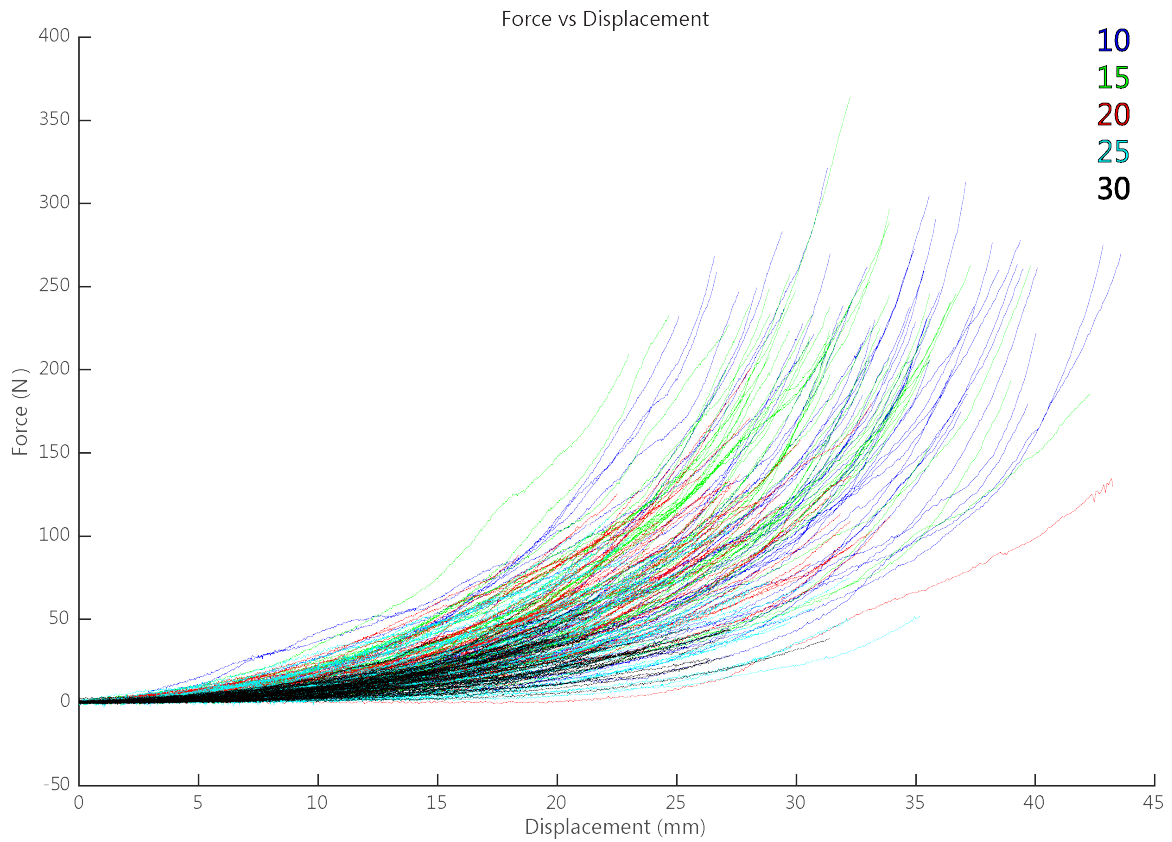
25	25	25	15	15	15	15	15	15	15
15	15	15	15	15	15	15	15	15	15
15	15	15	15	15	15	15	15	15	15
15	15	15	15	15	15	15	15	15	15
15	15	15	15	15	15	15	15	15	15
0	0	0	0	0	0	0	0	0	0
0	0	0	0	0	0	0	0	0	0
0	0	0	0	0	0	0	0	0	0
0	0	0	0	0	0	0	0	0	0
0	0	0	0	0	0	0	0	0	0

Samples	Group	P value should be
148-150	101-147	>0.95 P value actually is 0.18
Total Ridge Length		0.21
Area		0.22
Perimeter		0.02
Adjacency		
Samples	Group	P value should be
148-150	204-250	<0.05 P value actually is 0.87
Total Ridge Length		0.93
Area		0.9
Perimeter		0.04
Adjacency		
Samples	Group	P value should be
151-153	204-250	>0.95 P value actually is 0.27
Total Ridge Length		0.19
Area		0.22
Perimeter		0.37
Adjacency		
Samples	Group	P value should be
151-153	154-200	<0.05 P value actually is 0.04
Total Ridge Length		0.025
Area		0.022
Perimeter		0.39
Adjacency		
Samples	Group	P value should be
201-203	101-147	<0.05 P value actually is 0.65
Total Ridge Length		0.65
Area		0.57
Perimeter		0.71
Adjacency		
Samples	Group	P value should be
201-203	154-200	>0.95 P value actually is 0.41
Total Ridge Length		0.18
Area		0.14
Perimeter		0.97
Adjacency		

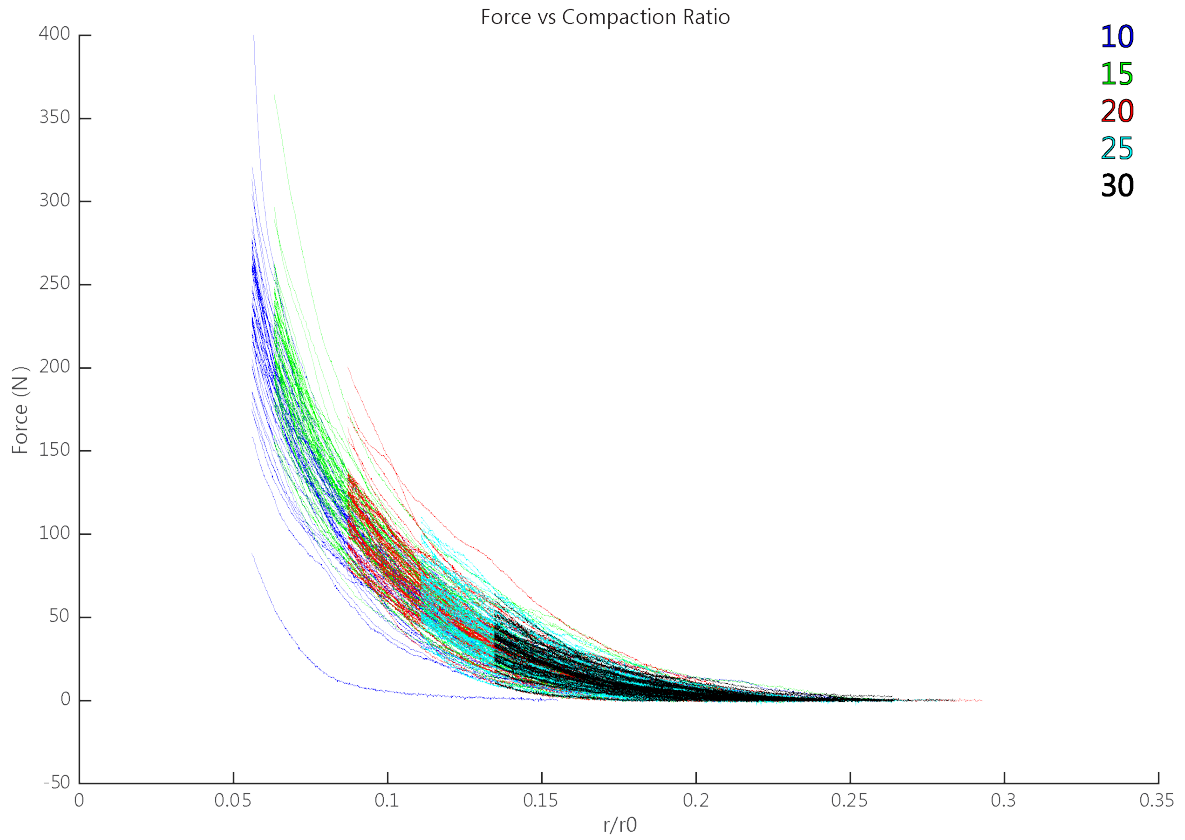
Thus, as almost all of the p-values were the opposite of what they were expected to be, it is reasonable to conclude that the samples had been switched.

11.4| COMPLETE PLOTS

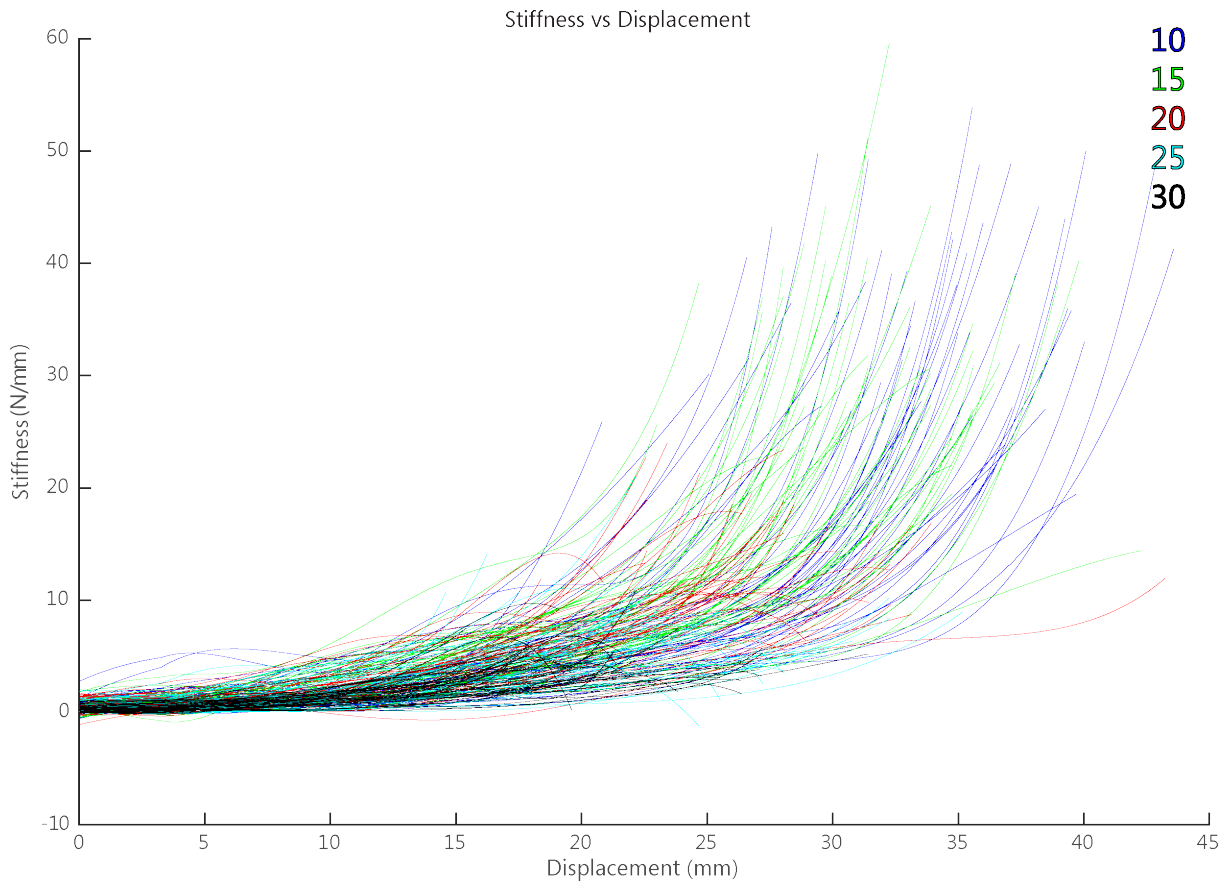
11.4.1| FORCE VS DISPLACEMENT



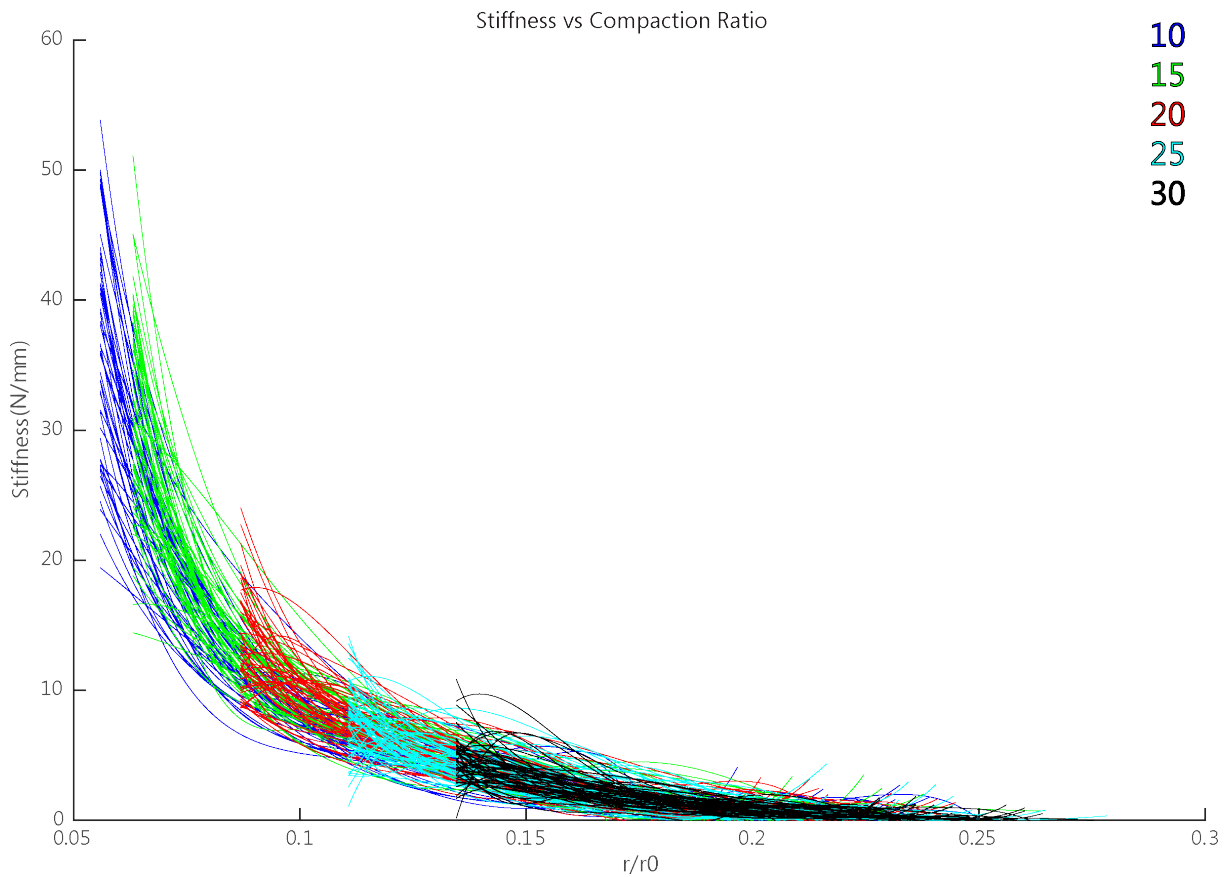
11.4.2| FORCE VS COMPACTION RATIO



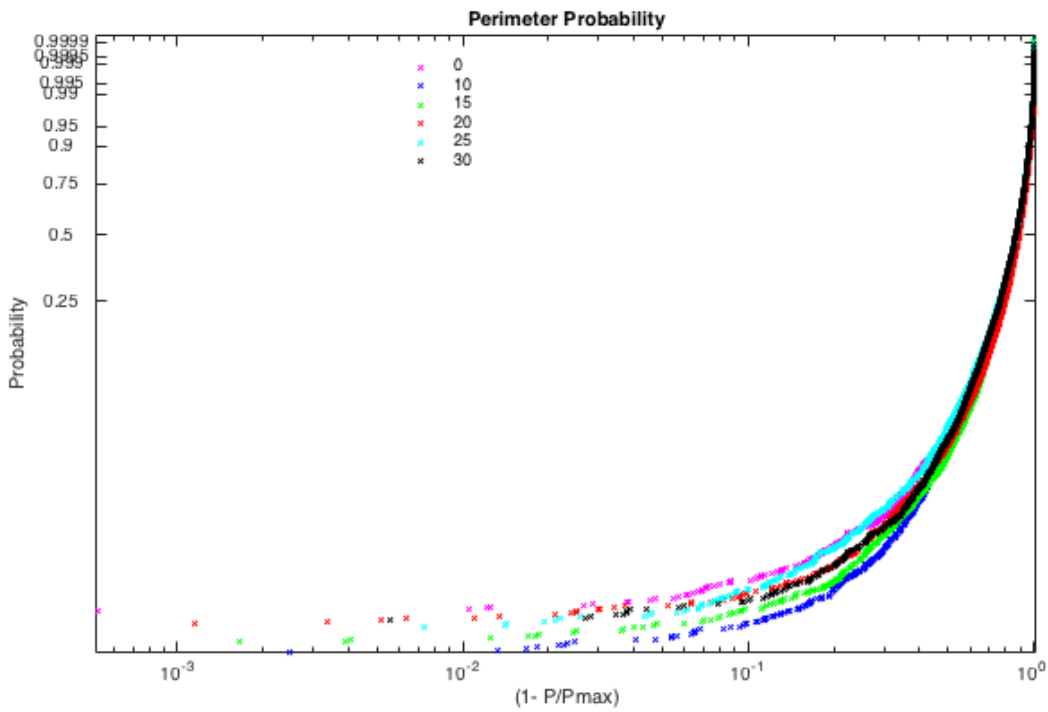
11.4.3| STIFFNESS VS DISPLACEMENT



11.4.4| STIFFNESS VS COMPACTION RATIO



11.5| PERIMETER PROBABILITY DISTRIBUTION



11.6| AREA PROBABILITY DISTRIBUTION

